Bioorganic Chemistry 143 (2024) 106984

Contents lists available at ScienceDirect

Bioorganic Chemistry

journal homepage: www.elsevier.com/locate/bioorg

Molecular hybrids of substituted phenylcarbamoylpiperidine and 1,2,4-triazole methylacetamide as potent 15-LOX inhibitors: Design, synthesis, DFT calculations and molecular docking studies

Zahid Nawaz [a], Naheed Riaz [a,*], Muhammad Saleem [a], Ambar Iqbal [a,b], Syeda Abida Ejaz [c], Bushra Bashir [a], Saima Muzaffar [d], Muhammad Ashraf [a,*], Aziz-ur-Rehman [e], Muhammad Sajjad Bilal [c], Bala Krishna Prabhala [f], Salvia Sajid [g]

[a] *Institute of Chemistry, Baghdad-ul-Jadeed Campus, The Islamia University of Bahawalpur, Bahawalpur 63100, Pakistan*
[b] *Department of Biochemistry, Institute of Biochemistry, Biotechnology and Bioinformatics (IBBB), Baghdad-ul-Jadeed Campus, The Islamia University of Bahawalpur, Bahawalpur 63100, Pakistan*
[c] *Department of Pharmaceutical Chemistry, Faculty of Pharmacy, Khawaja Fareed Campus, The Islamia University of Bahawalpur, Bahawalpur 63100, Pakistan*
[d] *Department of Chemistry, Division of Sceience and Technology, University of Education, 54770 Lahore, Vehari Campus, Pakistan*
[e] *Department of Chemistry, Government College University Lahore, Lahore 54000, Pakistan*
[f] *Institute of Physics, Chemistry and Pharmacy, University of Southern Denmark, Campusvej 55, 5230M, Denmark*
[g] *Department of Drug Design and Pharmacology, University of Copenhagen 2, DK-2100 Kobenhavn O, Denmark*

ARTICLE INFO

Keywords:
15-LOX inhibition
In silico studies
MTT assay
DFT calculations
ADME studies
Pipridinetriazole methylacetamides
Synthesis
Characterization

ABSTRACT

Inflammation is a multifaceted phenomenon triggered by potentially active mediators acutely released arachidonic acid metabolites partially in lipoxygenase (LOX) pathway which are primarily accountable for causing several diseases in humans. It is widely believed that an inhibitor of the LOX pathway represents a rational approach for designing more potent antiinflammatory leads with druggable super safety profiles. In our continual efforts in search for anti-LOX molecules, the present work was to design a new series of *N*-alkyl/aralkyl/aryl derivatives (**7a-o**) of 4-phenyl-5-(1-phenylcarbamoylpiperidine)-4*H*-1,2,4-triazole-3-thiol which was commenced in seriate formation of phenylcarbamoyl derivative (**1**), hydrazide (**2**), semicarbazide (**3**) and 4-phenyl-5-(1-phenylcarbamoylpiperidine)-4*H*-1,2,4-triazole-3-thiol (**4**). The aimed compounds were obtained by reacting 4-phenyl-5-(1-phenylcarbamoylpiperidine)-4*H*-1,2,4-triazole-3-thiol with assorted *N*-alkyl/aralkyl/aryl electrophiles. All compounds were characterized by FTIR, ^{1}H-, ^{13}C-NMR spectroscopy, EI-MS and HR-EI-MS spectrometry and screened against soybean 15-LOX for their inhibitory potential using chemiluminescence method. All the compounds except **7m** and **7h** inhibited the said enzyme remarkably. Compounds **7c, 7l**, **7j** and **7a** displayed potent inhibitions ranging from IC_{50} 1.92 ± 0.13 μM to 7.65 ± 0.12 μM. Other analogues **7g**, **7o**, **7e**, **7b**, **7d**, **7k** and **7n** revealed excellent inhibitory values ranging from IC_{50} 12.45 ± 0.38 μM to 24.81 ± 0.47 μM. All these compounds did not reveal DPPH radical scavenging activity. Compounds **7i-o** maintained > 90 % human blood mononuclear cells (MNCs) viability at 0.125 mM as assayed by MTT whilst others were found toxic. Pharmacokinetic profiles predicted good oral bioavailability and drug-likeness properties of the active scaffolds. SAR investigations showed that phenyl substituted analogue on amide side decreased inhibitory activity due to inductive and mesomeric effects while the mono-alkyl substituted analogues were more active than disubstituted ones and *ortho* substituted analogues were more potent than *meta* substituted ones. MD simulation predicted the stability of the **7c** ligand and receptor complex as shown by their relative RMSD (root mean square deviation) values. Molecular docking studies displayed hydrogen bonding between the compounds and the enzyme with Arg378 which was common in **7n**, **7g**, **7h** and baicalein. In **7a** and quercetin, hydrogen bonding was established through Asn375. RMSD values exhibited good inhibitory profiles in the order quercetin (0.73 Å) < **7 g** < baicalein < **7a** < **7n** < **7 h** (1.81 Å) and the binding free energies followed similar pattern. Density functional theory (DFT) data established good correlation between the active compounds and significant activity was associated with more stabilized LUMO (lowest unoccupied molecular orbitals) orbitals. Nevertheless, the present studies

* Corresponding authors.
E-mail addresses: nrch322@yahoo.com (N. Riaz), dr.m.ashraf@gmail.com (M. Ashraf).

https://doi.org/10.1016/j.bioorg.2023.106984
Received 27 September 2023; Received in revised form 8 November 2023; Accepted 17 November 2023
Available online 23 November 2023

declare active analogues like **7c, 7 l, 7a, 7j** as leads. Work is ongoing in derivatizing active molecules to explore more effective leads as 15-LOX inhibitors as antiinflammatory agents.

1. Introduction

Inflammation is a protracted evolved process linked with the activation, recruitment, and efficiency of innate as well as adaptive immune system cells. It is considered as a causal factor in the progression of several types of inflammatory diseases including cancer. Due to some external or internal stimuli, membrane phospholipids are hydrolyzed by phospholipase A_2 to liberate arachidonic acid and lysophosphatidic acid; the former on oxidation by two independent lipoxygenase (LOX) and cyclooxygenase (COX) pathways, yields biologically active mediators involved in the inflammatory processes [1]. LOX pathway is regulated by the rate limiting step carried out by 5-LOX, 12-LOX or 15-LOX, depending upon the number of double bond being oxidized to give 5-hydroperoxyeicosatetraenoic acid (5-HPETE), 12-HPETE, and 15-HPETE which further produce leukotrienes (LTs). 15-LOX is implemented in chronic bronchitis, asthma and cancer development [2,3]. The 12-HPETE interacts with G protein-coupled receptor in the PI3K/Akt/NF-κB pathway and increases the TNFα and IL-1β production which in turn increase reactive oxygen species (ROS) production. 5-LOX is involved in the synthesis of mediators implemented in bronchoconstrictor and several types of cancers [4–6].

The expression of 5-LOX and 12-LOX mRNA in four human pancreatic cancer cell lines (PANC-1, MiaPaca2, Capan2, and ASPC-1) was estimated by nested RT-PRC. The first type of 12-LOX, termed human platelet-type 12-LOX, accumulates in platelets, human erythroleukemia cells, and umbilical vein endothelial cells. The second type, porcine leukocyte-type 12-LOX, can metabolize both arachidonic acid and linoleic acid and can produce 12(*S*)-HETE and a trace amount of 15-(*S*)-HETE. The third type, called epithelium leukocyte-type 12-LOX and reticulocyte 15-lipoxygenase are both enzymes that catalyze the formation of 12(*S*)-HETE and 15(*S*)-HETE [5]. In humans, two types of 15-LOX have been identified: reticulocyte type 15-LOX-1 and epidermis type 15-LOX-2. In a rabbit reticulocyte mass, 15-LOX-1 was found as a single, 75-k_D polypeptide chain, while 15-LOX-2 was subsequently discovered in the human prostate, skin, and cornea.

The small molecules to be used as enzyme inhibitors are heterocycles containing nitrogen, sulfur or other heteroatoms. The design, synthesis and development of these bioactive molecules each with unique pharmacological properties is the most challenging [7]. In the last few decades, azolic derivatives like triazole, thiazole, thiadiazole and oxadiazole have attracted much attention because of their biological and synthetic importance and involvement in the formation of their fused heterocyclic-derived products [8]. Triazoles are five-member ring structures of three nitrogen atoms and their derivatives can interact easily towards various receptors and enzymes as hydrogen bond acceptors and donors resulting in a wide range of biological activities [9–11]. 1,2,4-Triazoles have garnered the attention because of their diverse pharmacological actions, minimal toxicities, powerful pharmacokinetic and pharmacodynamic features. Further, these molecules afford great variety of molecules, straight forward synthetic plans and usage in an array of combined analogues and non-fused scaffolds [8].

1,2,4-Triazole skeletons are incorporated in drugs including triazolam, estazolam, alprazolam (tranquillizer and anticonvulsant), fluconazole, itraconazole (antifungal), ribavirin (antiviral), anastrozole and rizatriptan (anti-migraine agents) and many others [12]. It is shown that the triazole ring can serve various weak interactions, including hydrophobic effects, coordination bonds, ion–dipole and hydrogen bonding providing a linker of pharmacophore with the targeted multiple binding sites [13]. In addition, 1,2,4-triazole nucleus exhibits stability against chemical and metabolic degradation. It can increase the solubility of the ligand and its polar nature can significantly enhance the pharmacokinetics and pharmacodynamics properties of the drug [8].

According to the pharmacodynamical principle of superposition, 1,2,4-triazole is a versatile scaffold reported to have potential pharmacological activities, such as anticancer [14], antifungal [15], antiurease [16], antiinflammatory [17], antioxidant [18] as well as anticonvulsant [19] properties. Currently, letrozole, anastrozole and vorozole are commonly used to treat estrogen-dependent breast cancer [20] (Fig. 1). Some derivatives of clotrimazole have been reported as antifungal agents [21]. Song et al synthesized a series of 4-*N*-nitrophenylsubstituted amino-4*H*-1,2,4-triazole derivatives as promising aromatase inhibitors [22] Further, Cevik et al explored a new benzimidazole-triazolothiadiazine hybrid with potent aromatase inhibitory activities [23]. Akhter et al reported a series of 1,2,4-triazole derivatives with potent inhibitory activity against the HepG2 cancer cell line [24].

In addition, Ouyang et al showed that a set of 1,2,4-triazole derivatives completely inhibited the tubulin polymerization by inducing cell cycle arrest at the G2/M phase of the A431 cell line [25]. Acetamide and azinane-bearing lead compounds are significant and essential pharmacophores of anticancer drugs [26]. Cefatrizine and tazobactam are triazole based antimicrobial and anticancer drugs, respectively. Therefore, 1,2,4-triazole nucleus can certainly provide avenues for researchers to find inventive potential drug candidates with more efficacy and selectivity [27].

1.1. Rationale of the work

Literature survey revealed that the piperidine analogues as vital components of the molecular structure of some important drugs in the treatment of various kinds of cancer, including cervical, pancreatic, colon, and breast cancer [28,29]. Piperidine carboxamide and the benzamide ring linked scaffolds are also found effective against SARS-CoV [30]. Triazole caffeic acid esters (**i-iii**) are found potent LOX inhibitors in sub-micromolar concentrations [31]. Compound (**iv**) with sulfone or sulfonamide groups also inhibited 5-LOX due to the involvement of hydrogen bonding and electrostatic interactions with various OH and NH functionalities of amino acids that supported the inhibitions [32]. Likewise, triazolylpyrazole oximes with sulfonamido derivative (**v**) showed potent inhibition (Fig. 2). The inhibitory potential compounds (**v,vi)** revealed that they fitted easily into the hydrophobic U-shaped pocket of the active site of the enzyme [33]. 4-Phenyl-1,2,4-triazole and *N*-(4-chlorophenyl)acetamide (**vii**) had various substituents (R = OMe, R_1 = Phenyl, R_2 = Cl) which increased the possibilities of hydrogen bonding and several hydrophobic interactions though the replacement of phenyl ring with an allyl group substantially decreased the binding affinity for 5-LOX [34]. Nevertheless, the conjugation of two or more biologically active scaffolds presents innovative hybrid pharmacophores with retained predetermined features. On this premise, earlier we synthesized and reported several pharmacologically active triazole and oxadiazole-based polyvalent derivatives (**viii-xi**) with acetamide functionalities as LOX inhibitors [35–42]. In the present study, triazole and propanamide hybrid pharmacophore with phenylcarbamoylpiperidine-4-carboxylate core was designed and derivatized decorated with hydrophobic aryl rings on each side of the triazole ring in search for potential leads as antiinflammatory agents (Fig. 2).

2. Results and discussion

2.1. Chemistry

In the present work, the synthesis of a new series of triazole

methylacetamides (**7a-o**) was carried out as described in Scheme 1 and further assessed for their *in vitro* enzyme inhibition potential against 15-LOX favored by cytotoxicity and *in silico* inquisition. Intending to reach the target compounds (**7a-o**), phenylisocyanate was first rubbed with isonepacotate (**a**) to get *N*-substituted ester (**1**), which was stirred with hydrazine hydrate and furnished hydrazide (**2**). Emergence of two singlets at δ 4.03 (1H, NH) and 8.92 in ^{1}H NMR spectrum of **2** endorsed the presence of $NHNH_2$ moiety. 4-Phenyl-(1-phenylcarbamoylpiperidine) thiosemicarbazide (**3**) was obtained when the hydrazide (**2**) was refluxed with phenyl isothiocyanate which was further refluxed in presence of 10 % NaOH, to get an intramolecular cyclized product, 4-phenyl-5-(1-phenylcarbamoylpiperidine)-4*H*-1,2,4-triazole-3-thiol (**4**). These interceders were recognized by ^{1}H NMR analysis, as *N*-phenyl nuclei resonated at δ 7.24 (5H, br s, *N*-Ph) in tandem with signals of phenyl carbamoyl moiety at δ 7.20 (1H, t, J = 7.5 Hz, H-4'), 7.42 (2H, t, J = 7.5 Hz, H-3',5'), 7.59 (2H, d, J = 7.5 Hz, H2',6') in spectrum of **3**. Besides, the C═S carbon nucleus reverberated at δ 179.7 in the ^{13}C-NMR spectrum of **3**, while, the peak for SH proton became visible at δ 11.3 in the ^{1}H NMR spectrum of compound **4**. Successful transformation of **3** into phenyl substituted 1,2,4-triazol-3-thiol (**4**) was confirmed by the absence of NH and carbonyl carbon signals in their respective NMR spectra. The alkyl/aralkyl/aryl amines (**5a-o**; Table 1) were stirred with 2-bromopropionyl bromide in a basic medium (pH 9–10) with the focus to get *N*-alkyl/aralkyl/aryl-2-bromopropanamides (**6a-o**), the other precursors of intended compounds. Finally, the targeted derivatives were procured by the coalescence of compound **4** separately with the precursors **6a-o**, respectively. The details of the procedures to achieve designed derivatives are laid out in the experimental section. Supplementary material.

The compound **7a** was synthesized as a white amorphous powder. The infrared (IR) spectrum showed the absorption bands at 3364, 3044, 2942, 1680, 1663, 1620–1543, 1262 for N—H, Ar-H, C—H, C═O, Ar-C═C, C═N, C—N functional groups, accordingly. In the ^{1}H NMR spectrum, two *N*-ethyl groups signaled at δ 1.06 (3H, t, J = 7.1 Hz, H-2""), 1.19 (3H, t, J = 7.1 Hz, H-2""), and 3.35 (4H, m, H-1"",1""), respectively. A doublet of methyl appeared at δ 1.62 (3H, d, J = 6.8 Hz, H-3"') allocated to the methyl group of linker amide. The resonating peaks at δ 1.78–1.98 (4H, m, H-3',5'), 2.71 (1H, m, H-4'), 2.88 (2H, m, H-2',6') and 4.03 (2H, m, H-2',6') advocated the presence of azinane ring bonded to 1,2,4-triazole. The methine of propanamide was detected by quartet arose at δ 4.97 (1H, q, J = 7.3 Hz, H-2"'). The peaks displayed at δ 7.29 (2H, m), 7.54 (3H, m) were allotted to the phenyl group attached to a nitrogen atom of triazole, whereas, a triplet and a multiplet signal exhibited at δ 7.00 (1H, t, J = 7.3 Hz, H-4"), 7.23 (4H, m, H-2",3",5",6") confirmed the presence of second phenyl group in the molecule. The BB and DEPT ^{13}C NMR spectra showed totally 23 carbon signals for 27 carbons which underpinned the presence of three methyl, six methylene, eight methine, and six quaternary carbon atoms. The most downfield peaks at δ 170.7, 155.0, 158.0, and 152.0 were assigned to two amide carbonyls and two quaternary carbons of triazole ring, respectively. The signal at δ 40.9 was corroborated for methine carbon atom linked to sulphur atom. The carbon signals at δ 43.8, 43.8, 29.9 and 29.8 substantiated the existence of azinane ring. The carbon atoms of *N*-ethyl groups resonated at δ 43.2, 42.8, 14.9, and 13.0. The signals at δ 139.1, 129.0, 123.2 and 120.1 were specified for the phenyl ring of phenylcarbamoyl moiety, while, the signals at δ 133.0, 130.5, 130.4, 127.3 were assigned to the phenyl bonded to triazole nucleus. The molecular formula $C_{27}H_{34}N_6O_2S$ of **7a** was established using HR-EI-MS which showed the molecular ion $[M]^+$ peak at m/z 456.2330. The structure elucidation of the remaining compounds **7b-o** of the series was composed in the same way and their spectral data is presented in the experimental section.

2.2. 15-LOX inhibitory activities and SAR studies

The SAR studies have provided insights into the structural characteristics that influenced the compounds inhibitory profiles against 15-LOX enzyme. The core structure of triazole itself has three nitrogens as heteroatoms and may exhibit different interactions with the enzyme's active site. Nonetheless, the substituents phenylcarbamoylpiperidine and methylacetamides having a variety of substituents on amide nitrogen can change the activity pattern of the compounds by variable interactions or differential inhibitory effects. *In vitro* 15-LOX inhibition of designed compounds 7a-o using quercetin (IC_{50} 4.86 ± 0.14 μM) and baicalein (IC_{50} 2.24 ± 0.13 μM) as references, and the activity data of the compounds are summarized as IC_{50} (Mean ± SEM) in Table 2.

As per our designing strategy to synthesize active moieties, all the compounds except 7 h and 7 m inhibited the 15-LOX activity wherein 7c, 7 l, **7j** and **7a** showed the potent inhibitions with IC_{50} 1.92 ± 0.13 μM, 3.29 ± 0.19 μM, 6.75 ± 0.34 μM and 7.65 ± 0.12 μM, respectively. Further, compounds 7 g, 7o, 7e, 7b, 7d, 7 k and 7n showed excellent inhibitory values with IC_{50} 12.45 ± 0.38 μM, 13.72 ± 0.38 μM, 17.26 ± 0.48 μM, 18.24 ± 0.45 μM, 19.25 ± 0.54 μM, 21.35 ± 0.45 μM, 24.81 ± 0.47 μM, respectively. Compounds 7i and 7f presented good inhibition against the enzyme with IC_{50} 31.95 ± 0.59 μM and 35.87 ± 0.69 μM, respectively (Fig. 3).

In this series (**7a-o**), four pharmacophoric groups are added for predictable interactions with the substrate binding site and possible hydrogen bonding with the oxygen and nitrogen atoms. The compound with the cyclohexyl substituted analogue 7c (IC_{50} 1.92 ± 0.13 μM) observed 13-fold higher activity than its structural analogue containing phenyl ring in 7o (IC_{50} 13.72 ± 0.38 μM), suggesting that the unsaturation of the ring caused a remarkable decrease in activity. This behavior can be justified based on the positive inductive effect of phenyl substituent, while the cyclohexyl had the positive mesomeric effect, thus enhancing the hydrogen bonding potential of the attached nitrogen atom. Inhibitory activities of 7a (IC_{50} 7.65 ± 0.12 μM) and 7b (IC_{50} 18.24 ± 0.45 μM) demonstrated that the diethyl groups in **7a** have intensified the charge density on nitrogen atom, increasing > 2-fold activity than propyl substitution in 7b. To further elucidating the effects

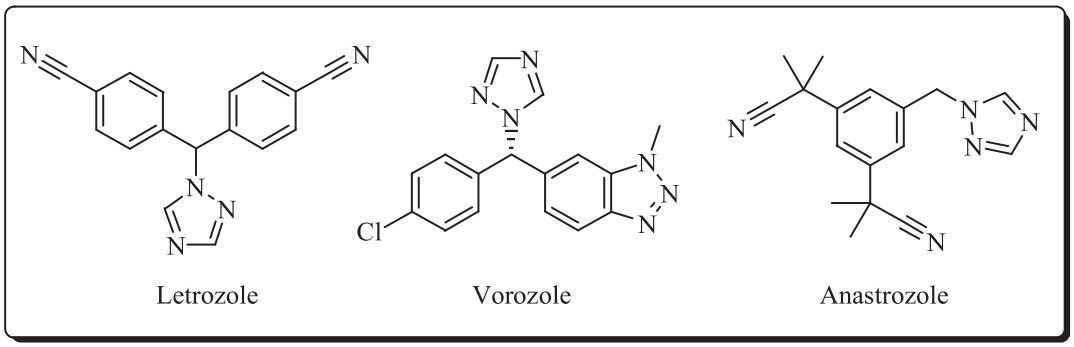

Fig. 1. Chemical structures of some 1,2,4-triazole based drugs.

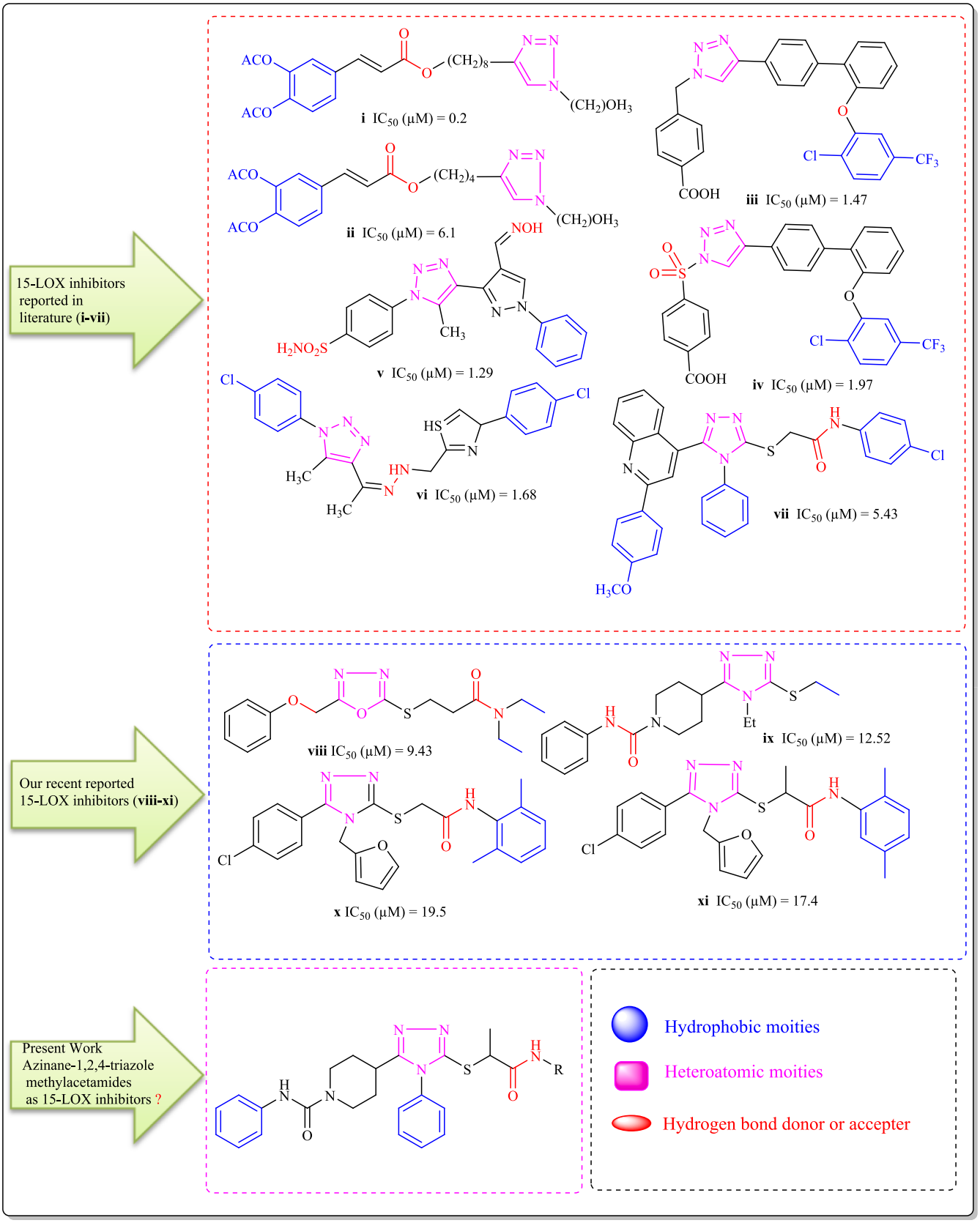

Fig. 2. Rationale of the current research plan and reported LOX inhibitors.

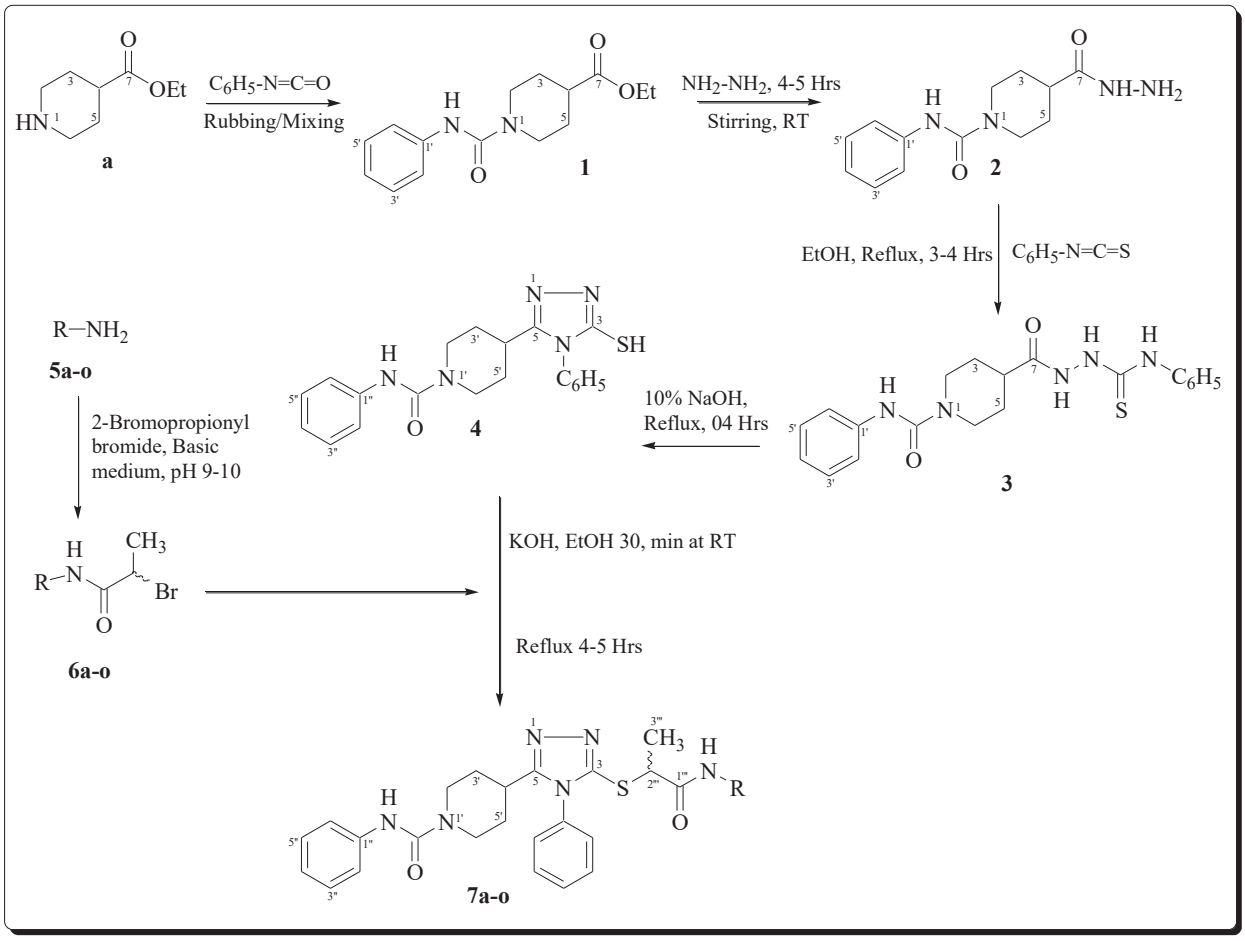

Scheme 1. Protocol for the synthesis of triazole amides (**7a-o**) from isonepacotate.

of the saturated alkyl substituents, we investigated the effects of substitutions at *ortho*, *meta*, and *para* positions on the phenyl group. A methyl functional group at the 2,4- (**7j**) and 2,6- (**7l**) positions of the benzene ring resulted in a significant increase in activity of compounds 7j and 7 l with IC_{50} 6.75 ± 0.34 μM and 3.29 ± 0.19 μM, respectively, in comparison with unsubstituted derivative 7o (IC_{50} 13.72 ± 0.38 μM); this effect may be due to the electron-donating nature of methyl groups, that is, in 7 l, both methyl groups are near to the nitrogen atom, increasing the potential of hydrogen bonding in 7 l than in 7j.

Analysis of other disubstituted compounds with methyl groups (7i, 7 k, 7n) reinforced the role of the substituents position on the activity. Equipotent compounds 7 k and 7n (IC_{50} 21.35 ± 0.45 μM and IC_{50} 24.81 ± 0.47 μM) have one methyl group at the same meta position, while the second methyl group at ortho (in 7 k) or meta (in 7n), causing a minor increase in activity of 7 k than 7n, because of the presence of ortho position near to nitrogen atom (Fig. 3). Activities of the monosubstituted derivatives (7e, 7f, 7 g, 7 h) also supported the SAR analysis as mentioned for disubstituted compounds. When collating the activities of 7e and 7 g (IC_{50} 17.26 ± 0.48 μM and 12.45 ± 0.38 μM), it is illustrated that the ethyl and methyl groups have comparable mesomeric effect. It is also displayed from the IC_{50} values of **7e** and **7f**, that *ortho* substituted derivative was more potent than *meta* substituted and same was true for **7g** and **7h**. From these investigations, it can be deliberated that the type and positions of substituents at the phenyl ring are of considerable significance in 15-LOX inhibitory activities (Fig. 3).

2.3. Cellular viability studies

Blood MNCs were employed for cytotoxic studies by MTT method at 0.125 mM concentration. Data in Table 2 shows that all the treated MNCs maintained their viability in the range from 73.56 ± 1.38 % to 98.75 ± 1.25 % and showed little toxicity as compared with the standard cytotoxic drugs at the same studied concentration. Compound **7g** displayed 73.56 ± 1.38 % viability under the experimental conditions and **7a** as 98.75 ± 1.25 % viability at 0.125 mM concentration.

2.4. Antioxidant activities

The DPPH radical scavenging activities of compounds **7a-o** were determined at 0.5 mM sample concentration along with the standard quercetin. All the compounds exhibited < 30 % antioxidant activity compared with the standard (83.61 ± 1.3 %) at this concentration.

2.5. ADME studies

The pharmacodynamics properties of the compounds **7a-o** were determined by MedChem Designer software ver. 3.0 (Table 3). The calculated properties of **7a-o** illustrate their druglikeness profiles. All compounds displayed good oral absorption properties as shown by their M logP, S + logP and S + logD values. The molecular weights of all compounds except one were > 500. The values of the number of rotatable bonds, molecular polar surface area and number of hydrogen bond donors are within the limits as predicted by the rule of five and Veber rule [43,44].

Successful drug absorption in the gastrointestinal tract (GIT) and penetration of the blood–brain barrier (BBB) are crucial for effective drug development. The boiled egg plot serves as a visual depiction illustrating the absorption and penetration processes within the GIT and

Table 1
Alkyl/aralkyl/aryl substituted amines.

Comp	R	Comp	R	Comp	R
a	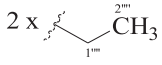	**f**	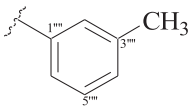	**k**	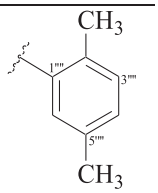
b	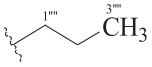	**g**	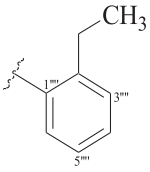	**l**	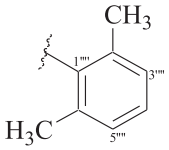
c	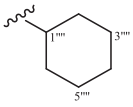	**h**	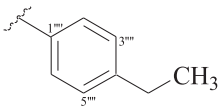	**m**	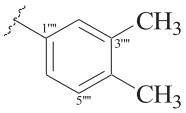
d	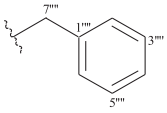	**i**	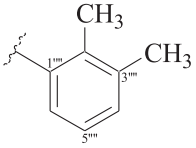	**n**	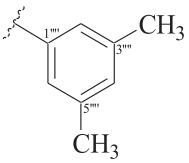
e	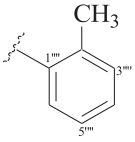	**j**	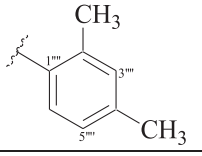	**o**	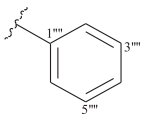

the BBB. The white portion of the egg represents the GIT absorption, while the yolk-like interior signifies the compound's passage through the BBB. Fig. 4 shows that the compounds **7a, 7b** and **7d** possess the ability to penetrate GIT and none of the analogues exhibited BBB penetration or GIT absorption. The poor GIT penetration hinders effective absorption and reduces therapeutic benefits while molecules unable to cross the BBB may fail to reach their CNS targets, hence leading to limited efficacy (Fig. 5).

2.6. Molecular docking studies

Protein crystal structure of 15-LOX from soybean (PDB ID: 1IK3, 2.0 Å) was downloaded and processed using Autodock and Biovia Discovery Studio [45–47]. Every heteroatom, including the co-crystal ligand, was eliminated from the protein and polar hydrogen atoms were added to get the protonated protein crystal. All the active ligands were docked into the active pocket of this 15-LOX protein using the built-in united atom scoring function with 10 runs for each ligand after protein and ligand preparation. The following amino acid residues make up the protein active pocket; Glu197, Arg260, Val26, Asp25, Val256, Lys278, Leu560, Leu563, Ala263, Phe272, Gln598, Asp592, Lys388, Asp 603, Tyr512, Asp431, Leu729, Gln574, Pro759, Gln762, Phe761, Thr443, Gly579, Arg580, Ile440, Trp578. During stiff receptor docking, the active pocket was considered to be static, allowing for prolonged interaction times between particular amino acid residues and chosen chemicals [46]. Finally, 2D and 3D poses were created, and best poses were selected for further investigations.

The antiinflammatory potential of **7c** and **7 l** was investigated by the docking manifestations. The results show that the derivatives **7c** and **7l** formed the most stable contacts and had the highest docking scores against the 15-LOX protein, −10.2 and −9.9 kcal/mol, respectively. The information gleaned from docking studies is compiled in Table 4.

2.6.1. Binding interaction of potent derivatives

The docking scores and binding interactions of all the derivatives (**7a-o**) were determined and visualized using Discovery studio and their 2D, 3D diagrams were generated. The results show that compound **7c** forms various stable bonding and non-bonding interactions with the following amino acids of the active pocket, i.e., Ser444, Thr443, Arg580, Ile440, Trp578, Gly579, Pro286, Leu285. Among all the binding interactions, two conventional hydrogen bonds and one carbon hydrogen bond is formed by the Ser444, Thr443 and Arg580 with the carbonyl oxygen atom and nearby benzene ring. The 3 π-alkyl contacts are established by the Ile440, Leu285 and Pro286 amino acid residues. All the π-anion interactions are also observed by the two benzene rings of both sides. The detailed interactions are illustrated Fig. 6.

Similarly, the docking interactions of compound **7l** are comparatively more stable among all the studied analogues (**7a-o**). The binding interactions of this compound include the amino acid residues, i.e., Gln762, Asn218, Thr443, Arg580, His219, Trp578, Ile440, Gly579, Pro759. The docking score of **7c** is slightly higher than **7l** which may be attributed to the addition of two methyl groups at the benzene ring. The bonding and non-bonding interactions of **7l** involve the formation of two conventional hydrogen bonds and two π-donor hydrogen bonds along with π-sigma and π-alkyl contacts. The two conventional hydrogen bonds are formed by the amino acids Asn218 and Gln762 with the

Table 2
15-LOX inhibitory, cytotoxicity profiles and antioxidant potential of compounds **7a-o** (Mean ± SEM, n = 3).

Comp	15-LOX assay Inhibition (%) at 0.25 mM	IC_{50} (μM)	MTT assay Cell viability (%) at 0.125 mM	Antioxidant activity (%) at 0.5 mM
7a	89.12 ± 1.27	7.65 ± 0.12	98.75 ± 1.25	13.6 ± 1. 2
7b	91.25 ± 1.24	18.24 ± 0.45	87.45 ± 1.43	14.3 ± 1.4
7c	93.15 ± 1.28	1.92 ± 0.13	78.76 ± 1.52	12.5 ± 1.6
7d	92.34 ± 1.35	19.25 ± 0.54	83.15 ± 1.27	12.8 ± 1.2
7e	91.23 ± 1.47	17.26 ± 0.48	92.76 ± 1.52	15.7 ± 1.5
7f	74.19 ± 1.25	35.87 ± 0.69	94.32 ± 1.47	16.3 ± 1.7
7 g	82.32 ± 1.46	12.45 ± 0.38	73.56 ± 1.38	23.5 ± 1.9
7 h	71.56 ± 1.24	52.63 ± 0.67	95.42 ± 1.51	21.4 ± 1.4
7i	87.13 ± 1.59	31.95 ± 0.59	92.75 ± 1.32	32.5 ± 1.6
7j	88.14 ± 1.63	6.75 ± 0.34	84.23 ± 1.43	18.2 ± 1.8
7 k	87.23 ± 1.46	21.35 ± 0.45	95.57 ± 1.23	28.5 ± 1.5
7 l	89.12 ± 1.39	3.29 ± 0.19	75.17 ± 1.34	16.3 ± 1.7
7 *m*	48.26 ± 1.42	> 250	96.58 ± 1.26	19.4 ± 1.8
7*n*	87.35 ± 1.23	24.81 ± 0.47	94.72 ± 1.27	13.9 ± 1.5
7o	84.12 ± 1.27	13.72 ± 0.38	91.35 ± 1.23	16.5 ± 1.6
Quercetin	96.63 ± 1.24	4.86 ± 0.14	–	83.61 ± 1.3
Baicalein	93.79 ± 1.27	2.24 ± 0.13	–	–
Cyclophosphamide	–	–	68.46 ± 1.95	–
Cisplatin	–	–	72.58 ± 1.93	–
Curcumin	–	–	73.92 ± 1.56	–

oxygen atom of both carbonyl groups. Correspondingly, two π-donor hydrogen linkages are observed by the amino acids Thr443 and Arg580 with the phenylpiperidine ring present in the center of the molecule. All other weak linkages are also observed with the same phenyl ring and Trp578, Ile440, Gly579, Pro759 (Fig. 7).

2.7. Density functional theory calculations

Using B3LYP functional theory and the 6-31G basis set, all the DFT calculations for the triazole derivatives (**7a-o**) were carried out as 6-32G is the most popular medium basis set for the atoms up to argon [48]. Gaussian software was used to determine the dipole moment, molecular polarizability, optimization energy, and numerous other characteristics [49]. The maximum stability of any chemical is linked to its lowest optimization energy, which may be reflected in its optimized structures. The most powerful compounds, **7c** and **7l**, optimized structures and frontier molecule orbitals (FMOs) are shown in the Fig. 8.

2.8. Frontier molecular orbitals

The energy of any compound for its highest occupied and lowest unoccupied molecular orbitals, or HOMO and LUMO, is used to determine the range of chemical properties related to its electronic distribution. Any derivative with a high HOMO value appears to be an excellent electron donor, and its electron acceptors property is reflected by its LUMO values [51]. The determination of local reactivity at various places in a compound is made easier with the help of the overall FMO calculations. A compound's HOMO/LUMO energy differential is a significant indicator to observe its reactivity profile. Any compound with a larger energy gap tends to be less reactive, as indicated by the high hardness value of the compound. All the compounds (**7a-o**) appear to be equally reactive based on the DFT calculations as shown by the nearly equal energy gap, E_{gap} = -0.168 eV, which is attributable to the similarity in the structural of the compound. The Table 5 lists several characteristics as well as the energy gap values for each compound (Table 6).

The behavior of reactive sites for any compound can be estimated by the value of its dipole moment, which is connected to the charge segregation in a molecule. The relative charge separation in a molecule is shown by the dipole moment's highest value for **7h**, i.e., 11.02 D, and the lowest for **7f** (4.80 D), respectively. The architectures of the HOMO and LUMO orbitals for the most potent compounds are shown in Fig. 9, while the polarizability, dipole moment, energy, and relative energy gaps are calculated and presented in Table 5, Fig. 10.

2.8.1. Chemical descriptors

The different parameters used to assess a compound's reactivity also include chemical hardness, chemical softness, electronegativity, electrophilicity index, and electronic chemical potential. The chemical formula (E_{LUMO}-E_{HOMO})/2) is used to determine the chemical hardness of a chemical system based on its stability and reactivity [52]. The ability of an atom in a molecule to draw electrons towards itself is known as electronegativity, which is quantified by the formula X = - (E_{HOMO} + E_{LUMO})/2). The electrophilicity index measures a molecule's capacity to accept electrons by utilizing its chemical hardness and electronic chemical potential. Table 5 contains the values of several chemical descriptors for all substances were determined and found similar.

2.8.2. Molecular dynamics simulations

The dynamic stability of the docked complex and the flexibility of the receptor protein were assessed using the MD simulation, an analytical technique that employs Newton's equations of motion. The LOX protein was in the most stable docking position when the protein–ligand complex of the **7c** derivative was simulated in aqueous conditions for 50 ns using NAMD software. Root mean square deviation (RMSD) and root mean square fluctuation (RMSF) data were utilized to forecast and analyze protein and behavior of the complex over the course of a trajectory.

For any complex, an RMSD value of < 2 is regarded as stable [50]. The score of **7c** ligand-receptor complex demonstrates its relative high behavior stability as compared to the value of the single protein. The ligand–protein complex remained in steady state throughout the whole process with minor changes along the trajectory as predicted by the RMSD values. The graphical representation of the ligand-receptor complex coupled with the RMSD and RMSF values is given in Fig. 8. The flexibility of protein residues is measured by RMSF values. RMSF is used in molecular dynamics simulations to identify protein areas that are more flexible than others. For instance, residues that participate in molecule-to-molecule interaction are frequently more flexible than other residues. The RMSF of our **7c** protein ligand complex indicate that the protein is relatively stable during simulation. The few amino acids are more flexible as indicated by the higher peaks in the graph.

3. Conclusions

In conclusion, a series of *N*-alkyl/aralkyl/aryl analogues (**7a-o**) of 4-phenyl-5-(1-phenylcarbamoylpiperidine)-4*H*-1,2,4-triazole-3-thiol was designed, synthesized, characterized and evaluated for inhibitory studies against soybean 15-LOX. Most of the compounds revealed

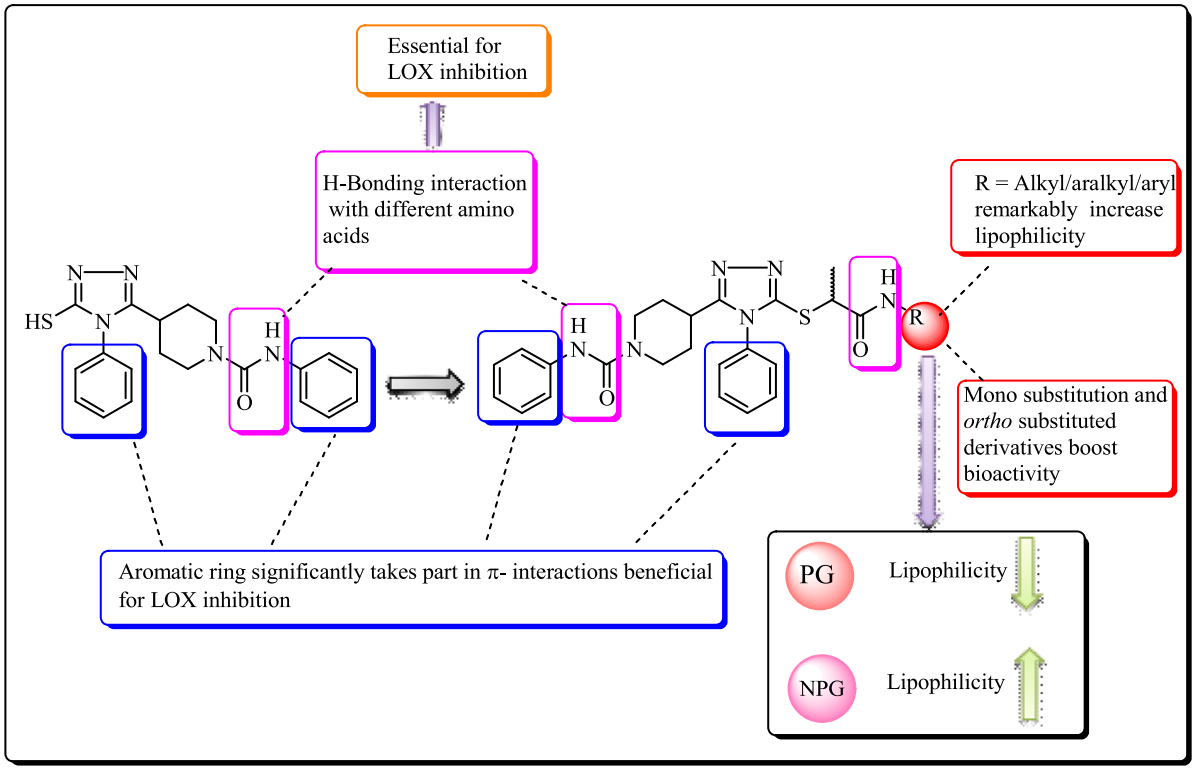

Fig. 3. Combined structure activity relationship (SAR) and docking study of **7a-o**.

Table 3
The calculated ADME properties of compounds **7a-o**.

Comp	MlogP	S + logP	S + logD	M. W.	M_NO	T_PSA	HBDH	nV
Lipinski/ Veber	**≤ 5**	**≤ 5**	**≤ 5**	**≤ 500**	**≤ 10**	**≤ 140 Å^2**	**≤ 5**	**≤ 1**
7a	3.815	3.244	3.244	506.674	8	83.360	1	1
7b	3.614	3.016	3.016	492.647	8	92.150	2	0
7c	4.209	3.910	3.910	532.712	8	92.150	2	1
7d	4.188	3.536	3.536	540.691	8	92.150	2	1
7e	4.456	4.076	4.076	540.691	8	92.150	2	1
7f	4.456	4.151	4.151	540.691	8	92.150	2	1
7 g	4.646	4.433	4.433	554.718	8	92.150	2	1
7 h	4.646	4.547	4.547	554.718	8	92.150	2	1
7i	4.646	4.396	4.396	554.718	8	92.150	2	1
7j	4.646	4.441	4.440	554.718	8	92.150	2	1
7 k	4.464	4.436	4.436	554.718	8	92.150	2	1
7 l	4.464	4.353	4.353	554.718	8	92.150	2	1
7 *m*	4.464	4.478	4.478	554.718	8	92.150	2	1
7*n*	4.464	4.509	4.509	554.718	8	92.150	2	1
7o	4.263	3.814	3.814	526.664	8	92.150	2	1
Quercetin	−0.235	1.958	1.529	302.242	7	131.36	5	0
Baicalein	1.296	3.019	2.823	270.243	5	90.9	3	0

Footnote: MlogP: Lipophilicity, M_NO: No. of rotatable bonds, T_PSA: Molecular polar surface area, HBDH: No. of H-bond donors, nV: No. of rule violations.

remarkable inhibitions against 15-LOX. Compounds **7c**, **7l**, **7j** and **7a** exhibited potent inhibitions from IC_{50} 1.92 ± 0.13 μM to 7.65 ± 0.12 μM and other derivatives **7g**, 7o, **7e**, **7b**, **7d**, **7k** and **7n** exposed excellent inhibitory profiles from IC_{50} 12.45 ± 0.38 μM to 24.81 ± 0.47 μM. These compounds did not show DPPH radical scavenging activity and observed less toxicity towards blood MNCs. The potent analogues displayed druglikeness features. The types and positions of substituents at the phenyl ring greatly influenced 15-LOX inhibitory activities. Mono-alkyl substituted analogues were comparatively more potent than the disubstituted and *ortho* substituted derivatives were more active than *meta* substituted ones. The reduced inhibitory activities in the unsaturated cyclohexyl substituted analogues was due to the intensive inductive and mesomeric effects. Compounds **7c** and **7l** were found most stable with lowest binding free energies of −10.2 and −9.9 kcal/mol, respectively, during the docking studies. Arg378 was involved in hydrogen bonding between the baicalein and **7n**, **7g**, **7h** and the receptor while Asn375 participated in hydrogen bonding in **7a** and quercetin. DFT calculations revealed that compounds with more stabilized LUMO orbitals were good inhibitors as predicted by *in vitro* data. The MD simulations of protein–ligand complex **7c** projected its stability of **7c** under 100 ns simulation. The data altogether demonstrates **7c, 7l, 7a, 7j** analogues as leads in search for 15-LOX inhibitors as antiinflammatory agents. Work is in progress in search for more analogues as potential leads.

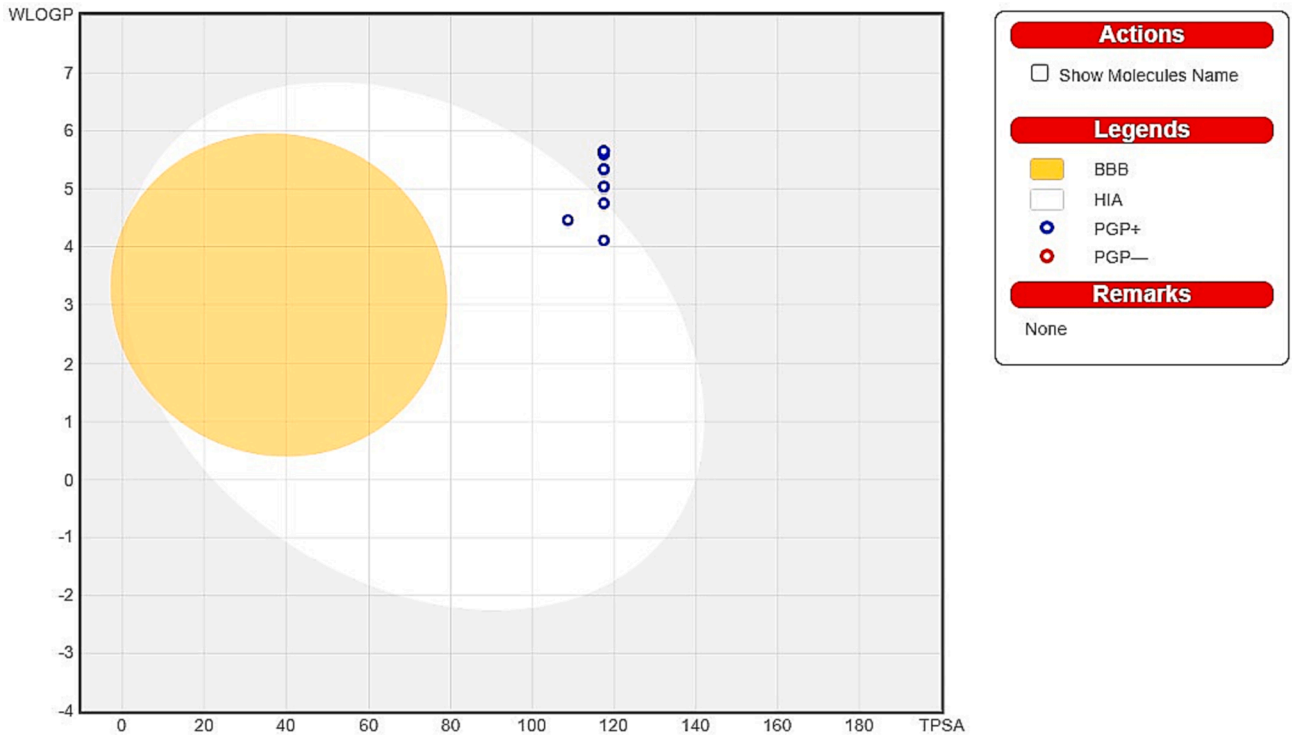

Fig. 4. Boiled egg plot depicting the human intestinal absorption (HIA) and blood brain barrier (BBB) penetration ability of the analogues. PGP in the graph indicate p-glycoprotein activation (+) or inhibition (-).

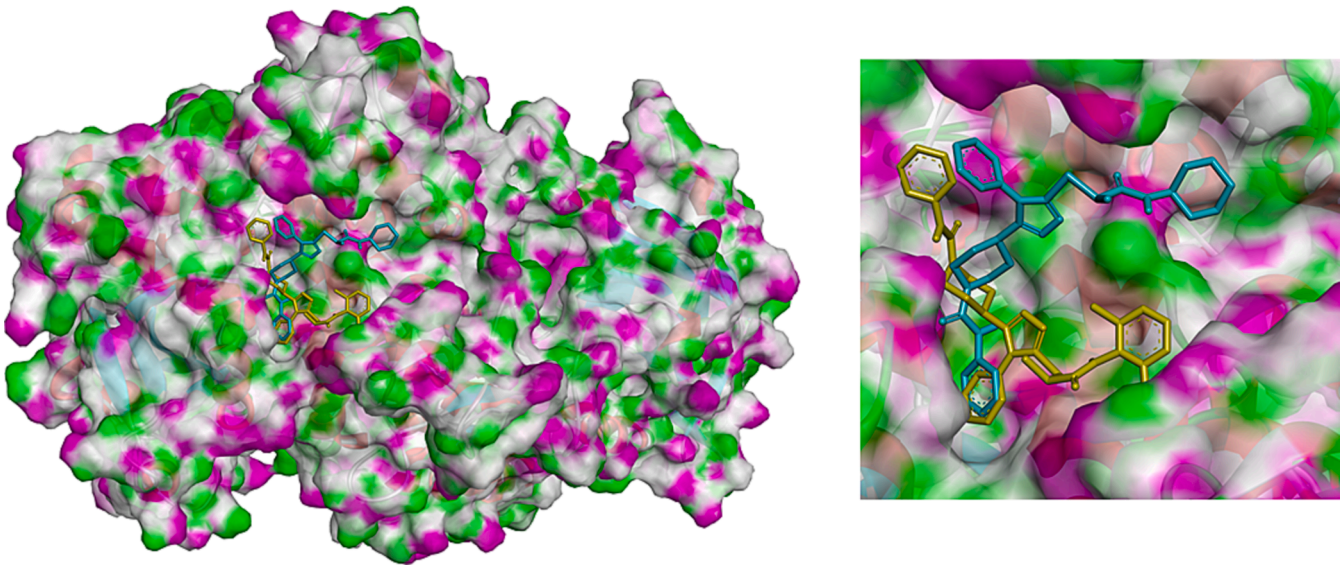

Fig. 5. Crystal structure of protein 15-LOX (PDB ID: 1IK3) and its active pocket with the ligands.

4. Experimental

4.1. Materials

All the chemicals and solvents of analytical grade were purchased from Sigma, Aldrich, and Alfa Aesar. The ^{1}H- and ^{13}C-NMR spectra were inscribed on Bruker instrument operating at 400 and 100 MHz, respectively, employing tetramethylsilane as an internal standard. IR spectra were obtained on Shimadzu 460 FTIR spectrometer as KBr pellets. The mass spectra were recorded on JMSA 500 mass spectrometer and JMS H × 110 spectrometer with a data system. Melting points were ascertained by using Gallen Kemp electrothermal apparatus.

4.2. Synthesis of ethyl 1-phenylcarbamoylpiperidine-4-carboxylate (*1*)

Phenyl isocyanate (0.025 mol, 2.98 mL) was trickled to ethyl piperidine-4-carboxylate (**a**; 0.025 mol, 3.8 mL) taken in a watch glass with incessant grinding, which continued (15–20 min) till the appearance of a single spot on TLC. The physical and spectroscopic data of compound **1** is given below: White solid; Yield: 97 %; M.P.: (104-109℃); IR (KBr, $\nu_{max,}$ cm^{-1}): 3397 (N—H), 3042 (Ar-H), 2951 (C—H), 1733, 1661 (C═O), 1614–1561 (Ar-C═C), 1262 (C—O, C—N); ^{1}H NMR (400 MHz, $CDCl_3$, ppm): δ 1.24 (3H, t, J = 7.0 Hz, $\underline{CH_3}$-CH_2-O), 2.12 (4H, m, H-3,5), 2.38 (1H, m, H-4), 3.59 (4H, m, H-2,6), 4.16 (2H, q, J = 7.0 Hz, CH_3-$\underline{CH_2}$-O), 7.07 (1H, t, J = 8.3 Hz, H-4'), 7.37 (2H, J = 8.3 Hz, H-3',5'),

Table 4
Binding free energy (kcal/mol) and molecular binding interactions displayed by ligand–protein complexes. Quercetin (*Q) and baicalein (*B) are standard inhibitors.

Comp	Binding free energy	Interaction type	Amino acid residues	RMSD (Å)
7a	−8.6	Hydrogen Bonding	Gln574, Arg731, Gln762, Thr443, Arg580	1.32
		Hydrophobic interactions	Leu729, Pro759, Gly579, Ile440, Trp578	
7b	−8.5	Hydrogen bonding	Gln762, Arg299, Thr443, Arg580, Glu573, Gln574	1.51
		Hydrophobic interactions	Gly579, Pro759, Trp578, Ile440,	
7c	−10.2	Hydrogen Bonding	Ser444, Thr443, Arg580	1.41
		Hydrophobic interactions	Ile440, Trp578, Gly579, Pro286, Leu285	
7d	−8.3	Hydrogen Bonding	Ser444, Arg731, Arg580, Thr443	1.28
		Hydrophobic interactions	Trp578, Ile440, Gly579, Leu729	
7e	−9.2	Hydrogen Bonding	Gln574, Arg580, Thr443, Gln762	0.45
		Hydrophobic interactions	Trp578, Gly579, Ile440, Arg731	
7f	−9.3	Hydrogen Bonding	Ser444, Thr443, Gln574, Arg580	0.98
		Hydrophobic interactions	Gly579, Ile440, Trp578, Leu285, Pro286	
7 g	−8.9	Hydrogen Bonding	Gln762, Arg580, Gly579	1.63
		Hydrophobic interactions	Arg299, Phe761, Pro759, Leu729,	
7 h	−8.7	Hydrogen bonding	Thr443, Ser444, Gln762	1.14
		Hydrophobic interactions	Phe761, Phe292, Glu573, Arg221, His219	
7i	−9.1	Hydrogen Bonding	Thr443, Arg580, Gln574	0.76
		Hydrophobic interactions	His219, Arg731, Pro759	
7j	−9.2	Hydrogen Bonding	Thr443, Arg580, Gln762	1.52
		Hydrophobic interactions	Phe761, Leu729, Ile440, Gly579	
7 k	−9.0	Hydrogen Bonding	Gln762, Arg580, Thr443, Ser444	1.93
		Hydrophobic interactions	Phe761, Leu729, Pro759, Gly579, Trp578, Ile440	
7 l	−9.9	Hydrogen Bonding	Gln762, Asn218, Thr443, Arg 580	0.42
		Hydrophobic interactions	His219, Trp578, Ile440, Gly579, Pro759,	
7 *m*	−9.6	Hydrogen Bonding	Ser444, Thr443, Arg580, Gln574	1.42
		Hydrophobic interactions	Gly579, Trp578, Pro286, Leu385	
7*n*	−9.4	Hydrogen Bonding	Thr445, Ser444, Thr443, Gln762	1.46
		Hydrophobic interactions	Phe761, Arg299, Pro759, Arg221, Glu573, His219	
7o	−9.1	Hydrogen bonding	Ser444, Thr443, Arg580, Gln574	1.21
		Hydrophobic interactions	Gly579, Ile440, Trp578, Leu285, Pro286	
***Q**	−8.47	Hydrogen bonding	Arg389, Asp608, Lys388, Asn375	1.13
		Hydrophobic interactions	Val589, Asp592, Asp390, Asp428, Leu,380	
***B**	−8.96	Hydrogen bonding	Asp431, Arg378, Leu376	1.53
		Hydrophobic interactions	Val594, Trp593, Leu520, Tyr512, Val589, Gln598, Cys379	

7.50 (2H, d, J = 8.3 Hz, H-2',6'); ^{13}C NMR (100 MHz, $CDCl_3$): δ 14.1 (CH_3), 28.5 (C-3,5), 40.4 (C-4), 46.5 (C-2,6), 61.6 (CH_2), 121.6 (C-2',6'), 128.0 (C-4'), 128.9 (C-3',5'), 139.4 (C-1'), 153.3 (C═O), 175.8 (COOEt); HR-EI-MS (m/z): 276.1491 $[M]^+$ calculated for $C_{15}H_{20}N_2O_3$; 276.1571.

4.3. Synthesis of 1-phenylcarbamoylpiperidine-4-carboxamide (2)

White fleecy precipitates of 1-phenylcarbamoylpiperidine-4-carboxamide (**2**) were synthesized when ethyl 1-phenylcarbamoylpiperidine-4-carboxylate (**1**; 0.024 mol, 6.7 g) was stirred for 4–5 h with 30 mL of hydrazine hydrate (80 %) in 100 mL round bottom flask. Precipitates were filtered, washed with cold distilled water, and dried. The physical and spectroscopic data of **2** is as follows: White shiny powder; Yield: 99 %; M.P.: (160–163 °C); IR (KBr, $\nu_{max,}$ cm^{-1}): 3385, 3353 (N—H), 3031 (Ar-H), 2948 (C—H), 1672, 1651 (C═O), 1617–1562 (Ar-C═C), 1239 (C—N); ^{1}H NMR (400 MHz, $CDCl_3$, ppm): δ 2.01 (4H, m, H-3,5), 2.49 (1H, m, H-4), 3.59 (4H, m, H-2,6), 7.07 (1H, t, J = 8.5 Hz, H-4'), 7.30 (2H, t, J = 8.5 Hz, H-3',5'), 7.58 (2H, d, J = 8.5 Hz, H-2',6'); ^{13}C NMR (100 MHz, $CDCl_3$): δ 29.4 (C-3,5), 40.1 (C-4), 47.0 (C-2,6), 121.6 (C-2',6'), 128.0 (C-4'), 128.9 (C-3',5'), 139.4 (C-1'), 153.5 (C═O), 178.2 (CONH); HR-EI-MS (m/z): 262.1449 $[M]^+$ calculated for $C_{13}H_{18}N_4O_2$; 262.1483.

4.4. Synthesis of 4-phenyl-(1-phenylcarbamoylpiperidine)thiosemicarbazide (3)

Phenyl isothiocyanate (2.63 mL, 0.022 mol) was added drop by drop with stirring to a 100 mL round bottom flask containing solution of compound **2** (5.9 g, 0.022 mol) using 30 mL of methanol as solvent. The mixture was refluxed and stirred for 3–4 h and the precipitates were formed on cooling which were filtered, washed and dried. Below is the physical and spectroscopic data of **3**: White powder; Yield: 97 %; M.P.: 181-185C; IR (KBr, $\nu_{max,}$ cm^{-1}): 3363 (N—H), 3032 (Ar-H), 2938 (C—H), 1677, 1662 (C═O), 1616–1551 (Ar-C═C), 1213 (C—N); ^{1}H NMR (400 MHz, $CDCl_3$, ppm): δ 2.01 (4H, m, H-3,5), 2.49 (1H, m, H-4), 3.59 (4H, m, H-2,6), 7.07 (1H, t, J = 8.5 Hz, H-4'), 7.25 (5H, br s, *N*-Ph), 7.30 (2H, t, J = 8.5 Hz, H-3',5'), 7.58 (2H, d, J = 8.5 Hz, H-2',6'); ^{13}C NMR (100 MHz, $CDCl_3$): δ 29.4 (C-3,5), 40.1 (C-4), 47.0 (C-2,6), 121.6 (C-2',6'), 128.0 (C-4'), 128.9 (C-3',5'), 139.4 (C-1'), *N*-Ph [126.5 (C-2,6), 128.6 (C-4), 127.8 (C-3,5), 134.5 (C-1)], 153.8 (C═O), 173.2 (CO), 181.5 (C═S); HR-EI-MS (m/z): 397.1593 $[M]^+$ calculated for $C_{20}H_{23}N_5O_2S$; 397.1570.

4.5. Synthesis of 4-phenyl-5-(1-phenylcarbamoylpiperidine)-4H-1,2,4-triazole-3-thiol (4)

In a 100 mL round bottom flask, compound **3** (0.021 mol, 8.5 g) was taken and dissolved in 10 % aqueous NaOH (30 mL) then refluxed for 4 h. After having single spot on TLC, the reaction mixture was poured into ice-cold water, pH 5–6 was attained using dilute HCl, precipitates were formed which were filtered, washed, and dried. The physical and spectroscopic data of **4** is as follows: White powder; Yield: 96 %; M.P.: 263-265C; IR (KBr, ν_{max}, cm^{-1}): 3367 (N—H), 3029 (Ar-H), 2931 (C—H), 1663 (C═O), 1617–1561 (Ar C═C, C═N), 1236 (C—N); ^{1}H NMR (400 MHz, $CDCl_3$, ppm): δ 2.01 (4H, m, H-3',5'), 2.49 (1H, m, H-4'), 3.59 (4H, m, H-2',6'), 7.07 (1H, t, J = 8.5 Hz, H-4"), 7.37 (2H, t, J = 8.5 Hz, H-3",5"), 7.50 (2H, d, J = 8.5 Hz, H-2",6"), 13.1 (1H, SH), *N*-Ph [7.41 (2H, m, H-2,6), 7.60 (3H, m, H-3–5)]; ^{13}C NMR (100 MHz, $CDCl_3$): δ

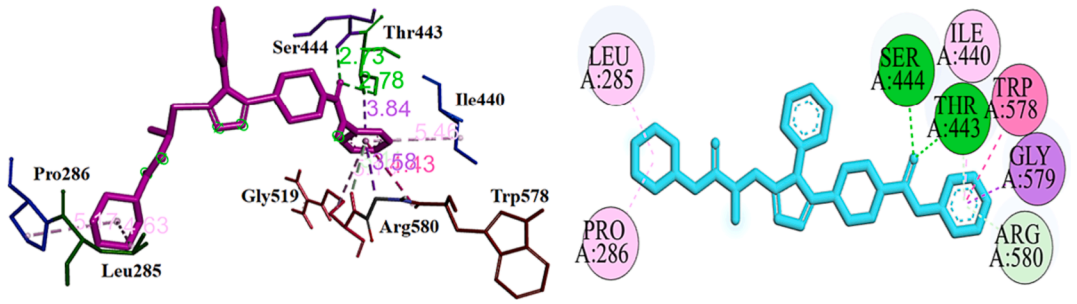

Fig. 6. 2D and 3D binding interactions of **7c** with in the active pocket of 15-LOX.

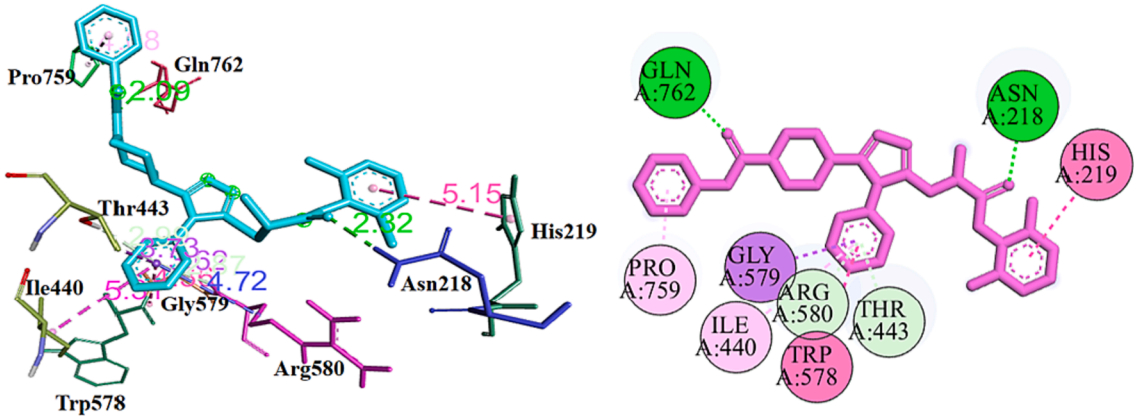

Fig. 7. 2D and 3D binding interactions of **7 l** with in the active pocket of 15-LOX.

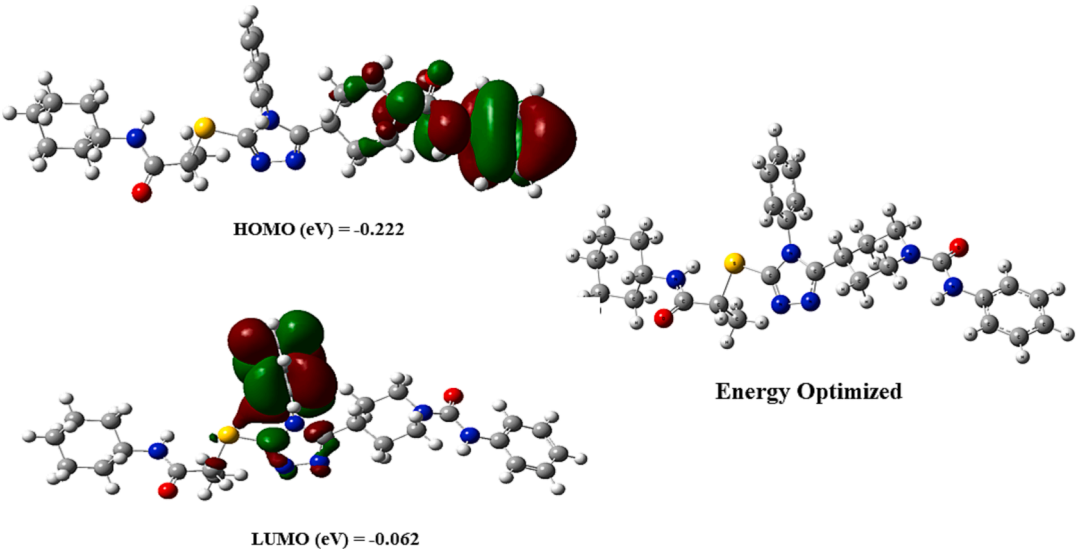

Fig. 8. Optimized structures along with HOMO and LUMO for **7c** using B3LYP/6-31G level of theory. Red, yellow and blue atoms indicate O, S and N atoms. Green color indicates electrophilic behavior and red color nucleophilic behavior. (For interpretation of the references to color in this figure legend, the reader is referred to the web version of this article.)

29.4 (C-3',5'), 40.1 (C-4'), 47.0 (C-2',6'), 121.6 (C-2",6"), 128.0 (C-4"), 128.9 (C-3",5"), 139.4 (C-1"), *N*-Ph [126.5 (C-2,6), 128.6 (C-4), 127.8 (C-3,5), 134.5 (C-1)], 153.8 (C═O), 173.2 (CO), 181.5 (C═S); HR-EI-MS (*m/z*): 379.1451 $[M]^+$ calculated for $C_{20}H_{21}N_5OS$; 379.1464.

4.6. *General procedure for the synthesis of compounds (**6a-o**)*

Computed amounts of alkyl/aralkyl/aryl amines (**5a-o**, 0.01 mol) were added separately in a quick fit Erlenmeyer flask containing 20 % aqueous Na_2CO_3 solution to sustain the pH 9–10. The bromopropionyl bromide (0.01 mol) was added slowly into the flask over 3–4 min with persistent vigorous shaking until the appearance of precipitates followed by stirring to get homogenous precipitates after 1–2 h. The solid product was filtered, washed with cold water, and dried to get the respective electrophile(s), *N*-alkyl/aralkyl/aryl substituted-2-bromopropanamides (**6a-o**).

Table 5
HOMO, LUMO and Optimization energies and their energy gaps.

Comp	Optimization Energy (eV)	Dipole moment (D)	Polarizability (α)	HOMO (eV)	LUMO (eV)	HOMO-LUMO (Δ eV)
7a	−1916.38	9.27	386.56	−0.221	−0.053	−0.168
7b	−1877.29	6.93	374.24	−0.222	−0.0534	−0.169
7c	−1993.40	7.04	406.33	−0.222	−0.053	−0.169
7d	−2028.88	9.25	407.77	−0.224	−0.062	−0.162
7e	−2028.88	6.22	419.35	−0.223	−0.055	−0.168
7f	−2028.67	4.80	360.89	−0.207	−0.034	−0.173
7 g	−2067.99	6.70	430.53	−0.223	−0.054	−0.169
7 h	−2067.75	11.35	391.32	−0.225	−0.065	−0.160
7i	−2067.99	10.22	432.95	−0.222	−0.055	−0.167
7j	−2067.99	10.90	389.22	−0.222	−0.054	−0.168
7 k	−2067.99	6.69	432.07	−0.223	−0.054	−0.169
7 l	−2067.99	6.34	430.62	−0.223	−0.055	−0.168
7 *m*	−2067.99	6.50	439.29	−0.222	−0.054	−0.168
7*n*	−2068.00	6.44	438.29	−0.223	−0.054	−0.169
7o	−1989.78	6.20	411.78	−0.223	−0.055	−0.168

Table 6
The calculated values of chemical descriptors for all scaffolds (**7a-o**).

Comp	Chemical Potential μ (eV)	Electronegativity X (eV)	Hardness η (eV)	softness S (eV-1)	Electrophilicity index ω (eV)
7a	−0.137	0.137	0.084	5.95	0.112
7b	−0.138	0.138	0.084	5.93	0.112
7c	−0.138	0.138	0.085	5.92	0.112
7d	−0.143	0.143	0.081	6.17	0.126
7e	−0.139	0.139	0.084	5.95	0.115
7f	−0.121	0.121	0.087	5.78	0.084
7 g	−0.139	0.139	0.085	5.92	0.114
7 h	−0.145	0.145	0.080	6.25	0.131
7i	−0.139	0.139	0.084	5.99	0.115
7j	−0.138	0.138	0.084	5.95	0.113
7 k	−0.139	0.139	0.085	5.92	0.114
7 l	−0.389	0.389	−0.166	−3.01	−0.456
7 *m*	−0.138	0.138	0.084	5.95	0.113
7*n*	−0.139	0.139	0.085	5.92	0.114
7o	−0.139	0.139	0.084	5.95	0.115

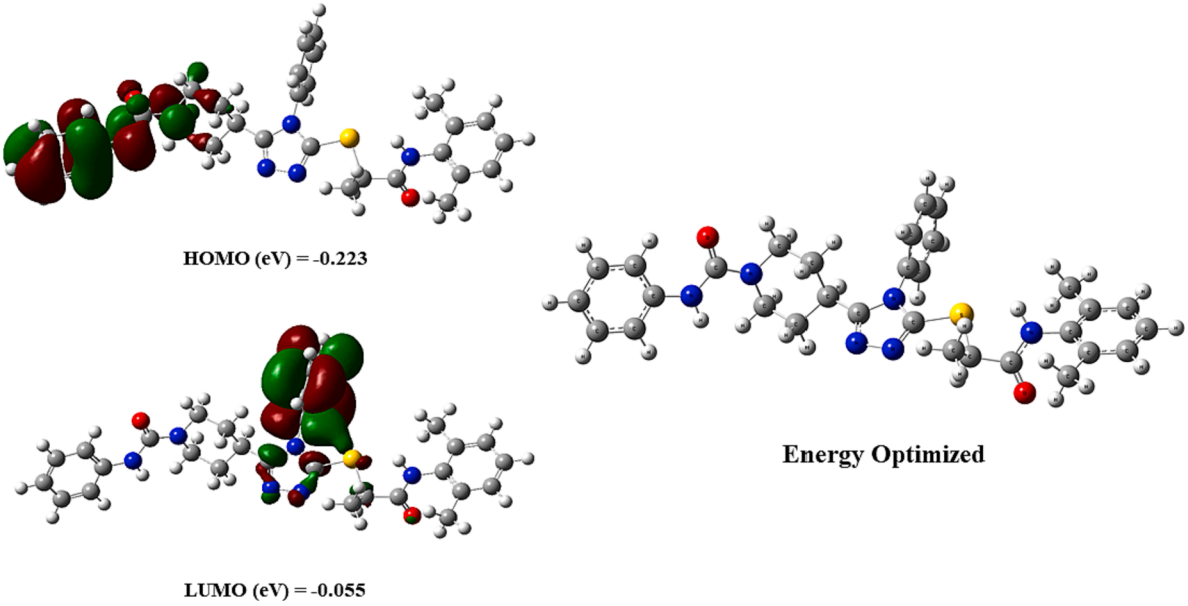

Fig. 9. Optimized structures along with the HOMO and LUMO orbitals for **7l** using B3LYP/6-31G level of theory. Red, yellow and blue atoms indicate O, S and N atoms. Green color indicates electrophilic behavior and red color nucleophilic behavior. (For interpretation of the references to color in this figure legend, the reader is referred to the web version of this article.)

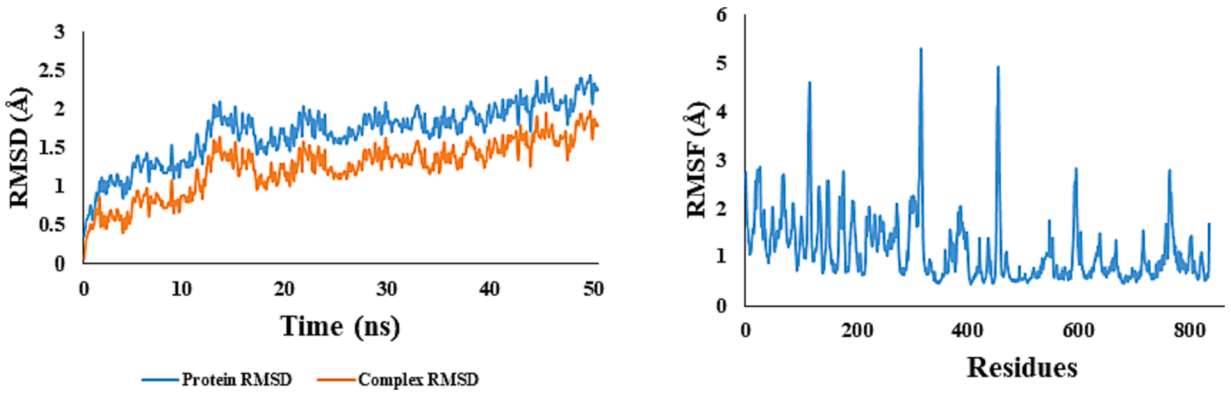

Fig. 10. Prediction of the dynamic stability of **7c** ligand–protein complex as expressed by their RMSD and RMSF values.

*4.7. General method for the synthesis of compounds (**7a-o**)*

Compound **4** (0.2 g, 0.5 mmol) was dissolved in 5 mL methanol followed by the addition of 30 mL ethanolic KOH (0.5 mmol) and the mixture was stirred for 30 min at room temperature. The electrophiles (**6a-o**), separately, were added slowly to the mixture and set to reflux for 4–5 h. An excess amount of cold distilled water was added to get the precipitates of the final products, **7a-o**, separately, which were filtered, washed, and dried.

*4.7.1. 2-(5-(1-Phenylcarbamoylpiperidine-4-yl)-4-phenyl-4H-1,2,4-triazol-3-ylthio)-N,N-diethylmethylacetamide (**7a**)*

White amorphous powder; Yield: 92 %; M.P.: 95-100℃; IR (KBr, ν_{max}, cm^{-1}): 3364 (N—H), 3044 (Ar-H), 2942 (C—H), 1680, 1663 (C═O), 1620–1543 (Ar-C═C, C═N), 1262 (C—N); ^{1}H NMR (400 MHz, $CDCl_3$): δ 1.07 (3H, t, J = 7.0 Hz, H-2""), 1.22 (3H, t, J = 7.0 Hz, H-2""), 1.62 (3H, d, J = 6.8 Hz, H-3""), 1.78–1.98 (4H, m, H-3',5'), 2.70 (1H, m, H-4'), 2.88 (2H, m, H-2',6'), 3.35 (3H, m, H-1"",1""), 3.58 (1H, m, H-1"",1""), 4.03 (2H, m, H-2',6'), 4.97 (1H, q, J = 6.8 Hz, H-2""), 7.00 (1H, t, J = 8.3 Hz, H-4"), 7.22–7.27 (4H, overlapped signal, H-2",3",5",6"), *N*-Ph [7.29 (2H, m, H-2,6), 7.54 (3H, m, H-3–5)]; ^{13}C NMR (100 MHz, $CDCl_3$): δ 13.0 (C-2""), 14.9 (C-2""), 20.1 (C-3""), 29.8 (C-5'), 29.9 (C-3'), 32.5 (C-4'), 40.9 (C-2""), 42.8 (C-1""), 43.2 (C-1""), 43.7 (C-6'), 43.8 (C-2'), 120.1 (C-2",6"), 123.2 (C-4"), 129.0 (C-3",5"), *N*-Ph [127.3 (C-2,6), 130.4 (C-3,5), 130.5 (C-4), 133.0 (C-1)], 139.1 (C-1"), 152.0 (C-3), 155.0 (C═O), 158.0 (C-5), 170.7 (C-1""); HR-EI-MS (*m/z*): 456.2330 $[M]^+$ calculated for $C_{27}H_{34}N_6O_2S$; 456.2307.

*4.7.2. 2-(5-(1-Phenylcarbamoylpiperidine-4-yl)-4-phenyl-4H-1,2,4-triazol-3-ylthio)-N-n-propylmethylacetamide (**7b**)*

White amorphous powder; Yield: 94 %; M.P.: 114-120℃; IR (KBr, $\nu_{max,}$ cm^{-1}): 3361 (N—H), 3034 (Ar-H), 2952 (C—H), 1681, 1660 (C═O), 1619–1541 (Ar-C═C, C═N), 1262 (C—N); ^{1}H NMR (400 MHz, $CDCl_3$): δ 0.84 (3H, t, J = 7.0 Hz, H-3""), 1.46–1.53 (2H, m, H-2""), 1.47 (3H, d, J = 7.0 Hz, H-3""), 1.50 (2H, m, H-2""), 1.78–1.98 (4H, m, H-3',5'), 2.73 (1H, m, H-4'), 2.88 (2H, m, H-2',6'), 3.18 (3H, t, J = 7.0 Hz, H-1""), 4.05 (2H, m, H-2',6'), 4.32 (1H, q, J = 7.0 Hz, H-2""), 7.01 (1H, t, J = 8.2 Hz, H-4"), 7.22–7.27 (4H, overlapped signal, H-2",3",5",6"), *N*-Ph [7.29 (2H, m, H-2,6), 7.57 (3H, m, H-3–5)]; ^{13}C NMR (100 MHz, $CDCl_3$): δ 11.4 (C-3""), 16.9 (C-3""), 22.7 (C-2""), 29.8 (C-5'), 29.9 (C-3'), 32.6 (C-4'), 41.6 (C-2""), 43.5 (C-1""), 43.7 (C-6'), 43.8 (C-2'), 120.1 (C-2",6"), 123.2 (C-4"), 127.2 (C-2"",6""), 129.0 (C-3",5"), *N*-Ph [127.2 (C-2,6), 130.5 (C-3,5), 130.8 (C-4), 132.7 (C-1)], 139.0 (C-1"), 152.5 (C-3), 154.9 (C═O), 158.0 (C-5), 170.6 (C-1""); HR-EI-MS (*m/z*): 492.2169 $[M]^+$ calculated for $C_{26}H_{32}N_6O_2S$; 492.2150.

*4.7.3. 2-(5-(1-Phenylcarbamoylpiperidine-4-yl)-4-phenyl-4H-1,2,4-triazol-3-ylthio)-N-cyclohexylmethylacetamide (**7c**)*

White amorphous powder; Yield: 92 %; M.P.: 208–220 C; IR (KBr, ν_{max}, cm^{-1}): 3352 (N—H), 3032 (Ar-H), 2956 (C—H), 1682, 1664 (C═O), 1624–1544 (Ar-C═C, C═N), 1260 (C—N); ^{1}H NMR (400 MHz, $CDCl_3$): δ 1.10–1.37 (4H, m, H-2"",3""), 1.46 (3H, d, J = 7.0 Hz, H-3""), 1.54 (2H, m, H-4""), 1.66–1.89 (5H, m, H-1"",5"",6""), 1.91–2.00 (4H, m, H-3',5'), 2.73 (1H, m, H-4'), 2.87 (2H, m, H-2',6'), 3.71 (1H, m, H-1""), 4.05 (2H, m, H-2',6'), 4.28 (1H, q, J = 7.0 Hz, H-2""), 7.00 (1H, t, J = 8.2 Hz, H-4"), 7.20–7.26 (2H, overlapped signal, H-2",3",5",6"), *N*-Ph [7.20–7.23 (2H, m, H-2,6), 7.56 (3H, m, H-3–5)]; ^{13}C NMR (100 MHz, $CDCl_3$): δ 16.8 (C-3""), 24.6 (C-3"",5""), 29.8 (C-5'), 30.0 (C-3'), 32.3 (C-4""), 32.6 (C-2"",6""), 32.7 (C-4'), 43.5 (C-2""), 43.8 (C-6'), 43.9 (C-2'), 48.4 (C-1""), 120.1 (C-2",6"), 123.2 (C-4"), 127.2 (C-2"",6""), 129.0 (C-3",5"), *N*-Ph [127.2 (C-2,6), 130.4 (C-3,5), 130.7 (C-4), 132.8 (C-1)], 139.1 (C = 1"), 152.2 (C-3), 155.0 (C═O), 158.0 (C-5), 170.3 (C-1""); HR-EI-MS (*m/z*): 532.2483 $[M]^+$ calculated for $C_{30}H_{38}N_6O_2S$; 532.2463.

*4.7.4. 2-(5-(1-Phenylcarbamoylpiperidine-4-yl)-4-phenyl-4H-1,2,4-triazol-3-ylthio)-N-benzylmethylacetamide (**7d**)*

White amorphous powder; Yield: 91 %; M.P.: 194-200℃; IR (KBr, ν_{max}, cm^{-1}): 3354 (N—H), 3038 (Ar-H), 2956 (C—H), 1681, 1661 (C═O), 1620–1540 (Ar-C═C, C═N), 1260 (C—N); ^{1}H NMR (400 MHz, CD_3OD): δ 1.52 (3H, d, J = 7.0 Hz, H-3""), 1.73–1.94 (4H, m, H-3',5'), 2.72 (1H, m, H-4'), 2.89 (2H, m, H-2',6'), 4.02 (2H, m, H-2',6'), 4.41 (3H, overlapped signal, H-2"",7""), 7.01 (1H, t, J = 8.2 Hz, H-4"), 7.22 (5H, m, H-2""-6""), 7.25 (4H, m, H-2",3",5",6"), *N*-Ph [7.30 (2H, m, H-2,6), 7.56 (3H, m, H-3–5)]; ^{13}C NMR (100 MHz, CD_3OD): δ 16.7 (C-3""), 29.8 (C-5'), 29.9 (C-3'), 32.5 (C-4'), 42.8 (C-2""), 43.6 (C-1""), 43.7 (C-6'), 43.8 (C-2'), 120.1 (C-2",6"), 123.2 (C-4"), 127.1 (C-5""), 127.2 (C-4"",6""), 127.7 (C-3"",7""), *N*-Ph [128.6 (C-2,6), 130.5 (C-3,5), 130.7 (C-4), 132.6 (C-1)], 138.6 (C-2""), 139.0 (C-1"), 152.4 (C-3), 155.0 (C═O), 158.0 (C-5), 171.4 (C-1""); HR-EI-MS (*m/z*): 540.2169 $[M]^+$ calculated for $C_{30}H_{32}N_6O_2S$; 540.2150.

*4.7.5. 2-(5-(1-Phenylcarbamoylpiperidine-4-yl)-4-phenyl-4H-1,2,4-triazol-3-ylthio)-N-(2-methylphenyl)methylacetamide (**7e**)*

White amorphous powder; Yield: 86 %; M.P.: 175-182℃; IR (KBr, ν_{max}, cm^{-1}): 3352 (N—H), 3037 (Ar-H), 2953 (C—H), 1680, 1665 (C═O), 1620–1530 (Ar-C═C, C═N), 1260 (C—N); ^{1}H NMR (400 MHz, $CDCl_3$): δ 1.58 (3H, d, J = 7.0 Hz, H-3""), 1.76–2.00 (4H, m, H-3',5'), 2.33 (3H, s, CH_3), 2.73 (1H, m, H-4'), 2.87 (2H, m, H-2',6'), 4.03 (2H, m, H-2',6'), 4.64 (1H, q, J = 7.0 Hz, H-2""), 7.02 (2H, overlapped signal, H-4",6""), 7.14 (2H, m, H-4"",5""), 7.24 (4H, m, H-2",3",5",6"), *N*-Ph [7.31 (2H, m, H-2,6), 7.57 (3H, m, H-3–5)], 8.01 (1H, d, J = 8.2 Hz, H-3""); ^{13}C NMR (100 MHz, $CDCl_3$): δ 16.5 (C-3""), 18.4 (CH_3), 29.9 (C-3'), 30.0 (C-5'), 32.6 (C-4'), 42.9 (C-2""), 43.7 (C-6'), 43.8 (C-2'), 120.1 (C-2",6"), 122.2 (C-2""), 123.3 (C-4"), 124.7 (C-5""), 127.1 (C-4""), 128.9 (C-3",5"), 129.0 (C-3""), *N*-Ph [126.6 (C-2,6), 130.5 (C-3,5), 130.6 (C-4), 132.5 (C-1)], 130.9 (C-2""), 136.5 (C-1""), 139.0 (C-1"), 152.7 (C-3), 155.0 (C═O), 158.3 (C-5), 169.7 (C-1""); HR-EI-MS (*m/z*): 540.2170 $[M]^+$ calculated for $C_{30}H_{32}N_6O_2S$; 540.2150.

4.7.6. 2-(5-(1-Phenylcarbamoylpiperidine-4-yl)-4-phenyl-4H-1,2,4-triazol-3-ylthio)-N-(3-methylphenyl)methylacetamide (7f)

White amorphous powder; Yield: 88 %; M.P.: 125-130℃; IR (KBr, ν_{max}, cm^{-1}): 3351 (N—H), 3034 (Ar-H), 2952 (C—H), 1681, 1662 (C═O), 1618–1525 (Ar-C═C, C═N), 1262 (C—N); ^{1}H NMR (400 MHz, $CDCl_3$): δ 1.56 (3H, d, J = 7.0 Hz, H-3'''), 1.79–1.99 (4H, m, H-3',5'), 2.32 (3H, s, CH_3), 2.74 (1H, m, H-4'), 2.88 (2H, m, H-2',6'), 4.07 (2H, m, H-2',6'), 4.50 (1H, q, J = 7.0 Hz, H-2'''), 6.89 (1H, d, J = 8.5 Hz, H-6''''), 7.02 (1H, t, J = 8.0 Hz, H-4''), 7.18 (1H, t, J = 8.5 Hz, H-5''''), 7.25 (4H, m, H-2'',3'',5'',6''), *N*-Ph [7.29 (2H, m, H-2,6), 7.57 (3H, m, H-3–5)]; 7.41 (1H, d, J = 8.5 Hz, H-4''''), 7.48 (1H, s, H-2'''), ^{13}C NMR (100 MHz, $CDCl_3$): δ 16.3 (C-3'''), 21.6 (CH_3), 29.8 (C-5'), 30.0 (C-3'), 32.6 (C-4'), 43.4 (C-6'), 43.4 (C-2'''), 43.9 (C-2'), 116.9 (C-2''''), 120.1 (C-2'',6''), 120.3 (C-6''''), 123.2 (C-4''), 123.3 (C-4''), 128.8 (C-5''''), 129.0 (C-3'',5''), *N*-Ph [124.9 (C-2,6), 130.5 (C-3,5), 130.9 (C-4), 138.4 (C-1)], 138.9 (C-1''''), 139.0 (C-1''), 152.9 (C-3), 154.9 (C═O), 158.1 (C-5), 169.3 (C-1'''); HR-EI-MS (m/z): 540.2170 $[M]^+$ calculated for $C_{30}H_{32}N_6O_2S$; 540.2150.

4.7.7. 2-(5-(1-Phenylcarbamoylpiperidine-4-yl)-4-phenyl-4H-1,2,4-triazol-3-ylthio)-N-(2-ethylphenyl)methylacetamide (7 g)

White amorphous powder; Yield: 90 %; M.P.: 94-105℃; IR (KBr, ν_{max}, cm^{-1}): 3351 (N—H), 3030 (Ar-H), 2952 (C—H), 1680, 1664 (C═O), 1618–1520 (Ar-C═C, C═N), 1261 (C—N); ^{1}H NMR (400 MHz, $CDCl_3$): δ 1.14 (3H, t, J = 7.1 Hz, $\underline{CH_3}$-CH_2), 1.58 (3H, d, J = 7.0 Hz, H-3'''), 1.77–1.99 (4H, m, H-3',5'), 2.60 (2H, q, J = 7.1 Hz, CH_3-$\underline{CH_2}$), 2.74 (1H, m, H-4'), 2.88 (2H, m, H-2',6'), 4.05 (2H, m, H-2',6'), 4.67 (1H, q, J = 7.0, H-2'''), 7.01 (1H, t, J = 8.2 Hz, H-4''), 7.07 (1H, t, J = 8.6 Hz, H-5''''), 7.18 (2H, m, H-4'''',6''''), 7.24 (4H, m, H-2'',3'',5'',6''), *N*-Ph [7.27 (2H, m, H-2,6), 7.55 (3H, m, H-3–5)], 7.90 (1H, d, J = 8.6 Hz, H-3''''); ^{13}C NMR (100 MHz, $CDCl_3$): δ 14.3 ($\underline{CH_3}$-CH_2-N), 16.5 (C-3'''), 24.7 (CH_3-$\underline{CH_2}$-N), 29.9 (C-5'), 30.0 (C-3'), 32.6 (C-4'), 42.9 (C-2'''), 43.7 (C-6'), 43.8 (C-2'), 120.1 (C-2'',6''), 123.3 (C-6''''), 123.4 (C-4''), 125.2 (C-4''''), 126.5 (C-3''''), *N*-Ph [127.1 (C-2,6), 130.6 (C-3,5), 130.8 (C-4), 135.4 (C-1)], 128.8 (C-5''''), 129.0 (C-3'',5''), 132.6 (C-2''''), 135.6 (C-1''''), 139.0 (C-1''), 152.8 (C-3), 155.0 (C═O), 158.3 (C-5), 169.8 (C-1'''); HR-EI-MS (m/z): 554.2325 $[M]^+$ calculated for $C_{31}H_{34}N_6O_2S$; 554.2307.

4.7.8. 2-(5-(1-Phenylcarbamoylpiperidine-4-yl)-4-phenyl-4H-1,2,4-triazol-3-ylthio)-N-(4-ethylphenyl)methylacetamide (7 h)

White amorphous powder; Yield: 96 %; M.P.: 100-104℃; IR (KBr, ν_{max}, cm^{-1}): 3350 (N—H), 3035 (Ar-H), 2960 (C—H), 1682, 1661 (C═O), 1616–1516 (Ar-C═C, C═N), 1260 (C—N); ^{1}H NMR (400 MHz, $CDCl_3$): δ 1.19 (3H, t, J = 7.2 Hz, $\underline{CH_3}$-CH_2), 1.55 (3H, d, J = 7.0 Hz, H-3'''), 1.77–1.99 (4H, m, H-3',5'), 2.58 (2H, q, J = 7.2 Hz, CH_3-$\underline{CH_2}$), 2.72 (1H, m, H-4'), 2.87 (2H, m, H-2',6'), 4.04 (2H, m, H-2',6'), 4.50 (1H, q, J = 7.0 Hz, H-2'''), 7.01 (1H, t, J = 8.2 Hz, H-4''), 7.12 (2H, d, J = 8.4 Hz, H-2'''',6''''), 7.24 (4H, m, H-2'',3'',5'',6''), *N*-Ph [7.26 (2H, m, H-2,6), 7.53 (3H, m, H-3–5)], 7.31 (2H, d, J = 8.4 Hz, H-3'''',5''''); ^{13}C NMR (100 MHz, $CDCl_3$): δ 15.9 ($\underline{CH_3}$-CH_2), 16.4 (C-3'''), 28.4 (CH_3-$\underline{CH_2}$), 29.8 (C-5'), 29.9 (C-3'), 32.6 (C-4'), 42.4 (C-2'''), 43.4 (C-6'), 43.8 (C-2'), 119.8 (C-2'''',6''''), 120.08 (C-2'',6''), 120.09 (C-3'''',5''''), 123.3 (C-4''), 128.3 (C-2'''',6''''), 129.0 (C-3'',5''), *N*-Ph [128.3 (C-2,6), 130.5 (C-3,5), 130.9 (C-4), 132.6 (C-1)], 136.2 (C-4''''), 139.0 (C-1'), 140.1 (C-1''''), 152.9 (C-3), 155.0 (C═O), 158.2 (C-5), 170.0 (C-1'''); HR-EI-MS (m/z): 554.2325 $[M]^+$ calculated for $C_{31}H_{34}N_6O_2S$; 554.2307.

4.7.9. 2-(5-(1-Phenylcarbamoylpiperidine-4-yl)-4-phenyl-4H-1,2,4-triazol-3-ylthio)-N-(2,3-dimethylphenyl)methylacetamide (7i)

White amorphous powder; Yield: 90 %; M.P.: 160-170℃; IR (KBr, ν_{max}, cm^{-1}): 3353 (N—H), 3037 (Ar-H), 2967 (C—H), 1683, 1667 (C═O), 1615–1515 (Ar-C═C, C═N), 1264 (C—N); ^{1}H NMR (400 MHz, $CDCl_3$): δ 1.58 (3H, d, J = 7.0 Hz, H-3'''), 1.77–1.97 (4H, m, H-3',5'), 2.19 (3H, s, CH_3), 2.27 (3H, s, CH_3), 2.73 (1H, m, H-4'), 2.87 (2H, m, H-2',6'), 4.04 (2H, m, H-2',6'), 4.64 (1H, q, J = 7.0, H-2'''), 6.95 (1H, d, J = 8.3 Hz, H-6''''), 7.01 (1H, t, J = 8.2 Hz, H-4''), 7.06 (1H, t, J = 8.3, H-5''''), 7.24 (4H, m, H-2'',3'',5'',6''), *N*-Ph [7.27 (2H, m, H-2,6), 7.57 (3H, m, H-3–5)], 7.68 (1H, d, J = 8.3 Hz, H-4''''); ^{13}C NMR (100 MHz, $CDCl_3$): δ 13.94 (CH_3), 16.5 (C-3'''), 20.8 (CH_3), 29.7 (C-5'), 30.0 (C-3'), 32.6 (C-4'), 43.1 (C-6'), 43.7 (C-2'''), 43.8 (C-2'), 120.1 (C-2'',6''), 121.1 (C-6''''), 123.2 (C-4''), 125.7 (C-4'''), 126.9 (C-5''''), *N*-Ph [127.2 (C-2,6), 130.5 (C-3,5), 130.8 (C-4), 136.1 (C-1)], 128.8 (C-3''''), 128.9 (C-3'',5''), 132.6 (C-2''''), 137.4 (C-1''''), 139.0 (C-1''), 152.7 (C-1), 154.9 (C═O), 158.3 (C-2), 169.8 (C-1'''); HR-EI-MS (m/z): 554.2325 $[M]^+$ calculated for $C_{31}H_{34}N_6O_2S$; 554.2307.

4.7.10. 2-(5-(1-Phenylcarbamoylpiperidine-4-yl)-4-phenyl-4H-1,2,4-triazol-3-ylthio)-N-(2,4-dimethylphenyl)methylacetamide (7j)

White amorphous powder; Yield: 89 %; M.P.: 88-100℃; IR (KBr, ν_{max}, cm^{-1}): 3349 (N—H), 3038 (Ar-H), 2970 (C—H), 1683, 1663 (C═O), 1611–1514 (Ar-C═C, C═N), 1265 (C—N); ^{1}H NMR (400 MHz, $CDCl_3$): δ 1.57 (3H, d, J = 7.0 Hz, H-3'''), 1.78–1.97 (4H, m, H-3',5'), 2.26 (3H, s, CH_3), 2.27 (3H, s, CH_3), 2.71 (1H, m, H-4'), 2.87 (2H, m, H-2',6'), 4.04 (2H, m, H-2',6'), 4.60 (1H, q, J = 7.0, H-2'''), 6.98 (1H, d, J = 8.1 Hz, H-6''''), 7.01 (1H, t, J = 8.2 Hz, H-4''), 7.24 (4H, m, H-2'',3'',5'',6''), 7.27 (1H, s, H-3''''), *N*-Ph [7.29 (2H, m, H-2,6), 7.58 (3H, m, H-3–5)], 7.82 (1H, d, J = 8.1 Hz, H-5''''); ^{13}C NMR (100 MHz, $CDCl_3$): δ 16.4 (C-3'''), 18.3 (CH_3), 29.9 (C-5'), 30.0 (C-3'), 32.6 (C-4'), 42.9 (C-6'), 43.7 (C-2'), 43.8 (C-2'), 120.1 (C-2'',6''), 122.4 (C-6''''), 123.3 (C-4''), 127.2 (C-5''''), 129.0 (C-3'',5''), 129.2 (C-3''''), *N*-Ph [127.1 (C-2,6), 130.5 (C-3,5), 130.8 (C-4), 133.9 (C-1)], 131.2 (C-4''''), 131.2 (CH_3), 132.5 (C-2''''), 134.4 (C-1''''), 139.0 (C-1''), 152.7 (C-1), 154.5 (C═O), 158.3 (C-2), 169.6 (C-1'''); HR-EI-MS (m/z): 554.2325 $[M]^+$ calculated for $C_{31}H_{34}N_6O_2S$; 554.2307.

4.7.11. 2-(5-(1-Phenylcarbamoylpiperidine-4-yl)-4-phenyl-4H-1,2,4-triazol-3-ylthio)-N-(2,5-dimethylphenyl)methylacetamide (7 k)

White amorphous powder; Yield: 94 %; M.P.: 175-182℃; IR (KBr, ν_{max}, cm^{-1}): 3355 (N—H), 3045 (Ar-H), 2968 (C—H), 1685, 1665 (C═O), 1614–1514 (Ar-C═C, C═N), 1266 (C—N); ^{1}H NMR (400 MHz, $CDCl_3$): δ 1.57 (3H, d, J = 7.0 Hz, H-3'''), 1.76–1.99 (4H, m, H-3',5'), 2.27 (3H, s, CH_3), 2.28 (3H, s, CH_3), 2.73 (1H, m, H-4'), 2.87 (2H, m, H-2',6'), 4.04 (2H, m, H-2',6'), 4.65 (1H, q, J = 7.0 Hz, H-2'''), 6.89 (1H, d, J = 8.6 Hz, H-4''''), 6.99 (1H, d, J = 8.6 Hz, H-3''''), 7.02 (1H, t, J = 7.2 Hz, H-4''), 7.26 (4H, m, H-2'',3'',5'',6''), *N*-Ph [7.29 (2H, m, H-2,6), 7.58 (3H, m, H-3–5)], 7.85 (1H, s, H-6''''); ^{13}C NMR (100 MHz, $CDCl_3$): δ 16.5 (C-3'''), 17.9 (CH_3), 21.2 (CH_3), 29.9 (C-5'), 30.0 (C-3'), 32.6 (C-4'), 42.9 (C-6'), 43.7 (C-2'''), 43.8 (C-2'), 120.1 (C-2'',6''), 123.2 (C-4''), 125.4 (C-6''''), 125.9 (C-4''''), *N*-Ph [125.9 (C-2,6), 130.5 (C-3,5), 130.9 (C-4), 136.2 (C-1)], 127.2 (C-3''''), 129.0 (C-3'',5''), 130.3 (C-5''''), 132.5 (C-2''''), 136.3 (C-1''''), 139.0 (C-1''), 152.7 (C-1), 154.9 (C═O), 158.3 (C-2), 169.7 (C-1'''); HR-EI-MS (m/z): 554.2523 $[M]^+$ calculated for $C_{31}H_{34}N_6O_2S$; 554.2307.

4.7.12. 2-(5-(1-Phenylcarbamoylpiperidine-4-yl)-4-phenyl-4H-1,2,4-triazol-3-ylthio)-N-(2,6-dimethylphenyl)methylacetamide (7 l)

White amorphous powder; Yield: 92 %; M.P.: 192-198℃; IR (KBr, ν_{max}, cm^{-1}): 3357 (N—H), 3040 (Ar-H), 2967 (C—H), 1680, 1666 (C═O), 1616–1517 (ArC = C, C═N), 1260 (C—N); ^{1}H NMR (400 MHz, CD_3OD): δ 1.65 (3H, d, J = 7.1 Hz, H-3'''), 1.81–1.92 (4H, m, H-3',5'), 2.13 (6H, s, CH_3), 2.83 (1H, m, H-4'), 3.34 (2H, m, H-2',6'), 4.17 (2H, m, H-2',6'), 4.69 (1H, q, J = 7.1 Hz, H-2'''), 7.07 (3H, m, H-3''''-5''''), 7.01 (1H, t, J = 8.3 Hz, H-4''), 7.25 (4H, m, H-2'',3'',5'',6''), *N*-Ph [7.33 (2H, m, H-2,6), 7.63 (3H, m, H-3–5)]; ^{13}C NMR (100 MHz, CD_3OD): δ 21.6 (2 × CH_3), 21.7 (C-3'''), 33.8 (C-5'), 33.9 (C-3'), 36.8 (C-4'), 47.6 (C-6'), 47.7 (C-2'), 48.7 (C-2'''), 124.9 (C-2'',6''), 126.9 (C-4''), 127.0 (C-5''''), 131.2 (C-4''''), 131.3 (C-3''''), *N*-Ph [131.9 (C-2,6), 134.5 (C-3,5), 134.8 (C-4), 139.4 (C-1)], 127.2 (C-3''''), 132.4 (C-3'',5''), 136.4 (C-2'''',6''''), 143.1 (C-1''''), 143.3 (C-1''), 152.7 (C-1), 154.9 (C═O), 158.3 (C-2), 169.7 (C-1'''); HR-EI-MS (m/z): 554.2523 $[M]^+$ calculated for $C_{31}H_{34}N_6O_2S$; 554.2307.

4.7.13. 2-(5-(1-Phenylcarbamoylpiperidine-4-yl)-4-phenyl-4H-1,2,4-triazol-3-ylthio)-N-(3,4-dimethylphenyl)methylacetamide (7 m)

White amorphous powder; Yield: 91 %; M.P.: 115-117℃; IR (KBr,

ν_{max}, cm^{-1}): 3353 (N—H), 3044 (Ar-H), 2966 (C—H), 1685, 1668 (C═O), 1617–1518 (Ar-C═C, C═N), 1264 (C—N); ^{1}H NMR (400 MHz, $CDCl_3$): δ 1.55 (3H, d, J = 7.0 Hz, H-3'''), 1.78–1.98 (4H, m, H-3',5'), 2.19 (3H, s, CH_3), 2.22 (3H, s, CH_3), 2.74 (1H, m, H-4'), 2.88 (2H, m, H-2',6'), 4.05 (2H, m, H-2',6'), 4.50 (1H, q, J = 7.0 Hz, H-2'''), 7.00 (1H, t, J = 8.4 Hz, H-4''), 7.05 (1H, s, H-2''''), 7.26 (4H, m, H-2'',3'',5'',6''), *N*-Ph [7.29 (2H, m, H-2,6), 7.57 (3H, m, H-3–5)], 7.34 (1H, dd, J = 8.1 Hz, H-5''''), 7.41 (1H, d, J = 8.1 Hz, H-6''''); ^{13}C NMR (100 MHz, $CDCl_3$): δ 16.4 (C-3'''), 19.3 (CH_3), 19.9 (CH_3), 29.8 (C-5'), 32.7 (C-4′), 36.0 (C-3'), 43.4 (C-6'), 43.8 (C-2'''), 43.9 (C-2'), 117.2 (C-2''''), 120.1 (C-2'',6''), 121.0 (C-6''''), 123.3 (C-4''), *N*-Ph [127.2 (C-2,6), 130.5 (C-3,5), 130.8 (C-4), 136.2 (C-1)], 129.0 (C-3'',5''), 130.0 (C-5''''), 130.8 (C-4''''), 132.4 (C-4''''), 132.6 (C-3''''), 137.2 (C-1'''), 139.0 (C-1''), 152.8 (C-3), 154.9 (C═O), 158.1 (C-5), 169.1 (C-1'''); HR-EI-MS (*m/z*): 554.2325 $[M]^+$ calculated for $C_{31}H_{34}N_6O_2S$; 554.2307.

4.7.14. 2-(5-(1-Phenylcarbamoylpiperidine-4-yl)-4-phenyl-4H-1,2,4-triazol-3-ylthio)-N-(3,5-dimethylphenyl)methylacetamide (**7n**)

White amorphous powder; Yield: 89 %; M.P.: 144-150℃; IR (KBr, ν_{max}, cm^{-1}): 3353 (N—H), 3043 (Ar-H), 2968 (C—H), 1682, 1666 (C═O), 1617–1518 (Ar-C═C, C═N), 1261 (C—N); ^{1}H NMR (400 MHz, $CDCl_3$): δ 1.54 (3H, d, J = 7.0 Hz, H-3'''), 1.78–1.99 (4H, m, H-3',5'), 2.27 (6H, s, CH_3), 2.73 (1H, m, H-4'), 2.89 (2H, m, H-2',6'), 4.07 (2H, m, H-2',6'), 4.50 (1H, q, J = 7.0, H-2'''), 6.39 (1H, s, H-4''''), 6.71 (2H, s, H-2'''',6''''), 7.01 (1H, t, J = 8.2 Hz, H-4''), 7.25 (4H, m, H-2'',3'',5'',6''), *N*-Ph [7.29 (2H, m, H-2,6), 7.57 (3H, m, H-3–5)]; ^{13}C NMR (100 MHz, $CDCl_3$): δ 16.4 (C-3'''), 21.4 (2 × CH_3), 29.9 (C-5'), 30.0 (C-3'), 32.7 (C-4'), 43.5 (C-6'), 43.9 (C-2'), 43.9 (C-2'''), 117.5 (C-2'''',6''''), 120.1 (C-2'',6''), 123.3 (C-4''), 125.9 (C-4''''), *N*-Ph [127.1 (C-2,6), 130.5 (C-3,5), 130.9 (C-4), 138.3 (C-1)], 129.0 (C-3'',5''), 130.9 (C-4''''), 132.6 (C-3'''',5''''), 138.7 (C-1''''), 139.0 (C-1''), 152.8 (C-3), 154.9 (C═O), 158.2 (C-5), 169.3 (C-1'''); HR-EI-MS (*m/z*): 554.2325 $[M]^+$ calculated for $C_{31}H_{34}N_6O_2S$; 554.2307.

4.7.15. 2-(5-(1-Phenylcarbamoylpiperidine-4-yl)-4-phenyl-4H-1,2,4-triazol-3-ylthio)-N-phenylmethylacetamide (**7o**)

White amorphous powder; Yield: 90 %; M.P.: 210-213℃; IR (KBr, ν_{max}, cm^{-1}): 3351 (N—H), 3035 (Ar-H), 2955 (C—H), 1680, 1661 (C═O), 1618–1519 (Ar-C═C, C═N), 1260 (C—N); ^{1}H NMR (400 MHz, CD_3OD): δ 1.59 (3H, d, J = 7.1 Hz, H-3'''), 1.72–1.94 (4H, m, H-3',5'), 2.79 (1H, m, H-4'), 3.34 (2H, m, H-2',6'), 4.15 (2H, m, H-2',6'), 4.48 (1H, q, J = 7.1 Hz, H-2'''), 7.0 (1H, t, J = 8.3 Hz, H-4''), 7.10 (2H, t, J = 8.4 Hz, H-3'''',5''''), 7.25 (1H, t, J = 8.4 Hz, H-4''''), 7.30 (4H, m, H-2'',3'',5'',6''), 7.50 (2H, d, J = 8.4 Hz, H-2'''',6''''), *N*-Ph [7.27 (2H, m, H-2,6), 7.58 (3H, m, H-3–5)]; ^{13}C NMR (100 MHz, CD_3OD): δ 17.8 (C-3'''), 20.3 (C-5'), 30.4 (C-3'), 33.4 (C-4'), 44.2 (C-6'), 44.2 (C-2'''), 45.7(C-2'), 120.3 (C-2'''',6''''), 121.3 (C-2'',6''), 123.5 (C-4''), 124.9(C-4''''), 128.9 (C-3'',5''), 129.3 (C-3'''',5''''), *N*-Ph [127.7 (C-2,6), 130.8 (C-3,5), 131.3 (C-4), 132.8 (C-1)], 138.5 (C-1''''), 139.8 (C-1''), 152.5 (C-3), 156.7 (C═O), 159.1 (C-5), 170.3 (C-1'''); HR-EI-MS (*m/z*): 526.2014 $[M]^+$ calculated for $C_{29}H_{30}N_6O_2S$; 526.1994.

4.8. 15-LOX inhibition assay

The 15-LOX inhibition assay was carried out as reported earlier [39,41]. Briefly, a total volume of 100 μL reaction mixture contained 60 μL of 200 mM borate buffer pH 9.0, 10 μL of test solution and 10 μL soybean 15-LOX solution. After mixing and pre-incubation for 5 min at 25℃, 10 μL of 3 nM luminol containing 1 nM cytochrome *c* solution was pipetted in the reaction well. Reaction was started by the addition of 10 μL substrate linoleic acid solution. The relative counts were measured from 100 to 300 s by 96-well plate Synergy HTX BioTek USA. All experiments were carried out in triplicates with negative and positive controls. The active test solutions were suitably diluted and assayed to determine their percentage inhibitions and data was used for the determination of IC_{50} values.

4.9. MNCs cell viability assay

Cell viability assay was performed using blood mononuclear cells (MNCs) method as reported [39,41]. Briefly, human blood was taken from healthy volunteer with consent and MNCs were isolated using density gradient Lymphocyte Separation Medium of density 1.077 g/mL. MNCs were collected at the interface and washed and suspended in 50 mM phosphate buffer saline, pH 7.4 (PBS). The assay contents contained PBS, 20 μL test solution and 40 μL MNCs (20,000–30,000 cells) in the 96 well plate. The contents were incubated for 2 h at 37C followed by the addition of 10 μL 3-(4,5-dimethylthiazol-2-yl)-2,5-diphenyltetrazoliumbromide)tetrazolium solution (MTT, 5 mg/mL). After 18–20 h incubation at 37C, 100 μL DMSO was added to make 200 μL volume. The contents were further incubated for 2 h and absorbance read at 540 nm. All test solutions along with positive and negative controls were used in triplicates and data was expressed as Mean ± SEM, n = 3.

4.10. . Antioxidant assay

Antioxidant assay was carried out by the method reported [53]. The reaction mixture of 100 μL involved 10 μL of test solution (0.5 mM) and 90 μL of 0.5 mM DPPH solution in methanol in 96-well plate. The contents were mixed and incubated for 20–25 min in the dark at 30 °C. Absorbance was measured at 517 nm. Assays were done in triplicates with both positive (quercetin) and negative controls and data was expressed as Mean ± SEM, n = 3.

4.11. . Computational analysis

4.11.1. Molecular docking

To perform molecular docking, the protein crystal structure of 15-LOX from soybean (PDB ID: 1IK3, 2.0 Å) was downloaded from RCSB protein data bank and processed using Autodock and Biovia Discovery Studio [54]. Every heteroatom, including the co-crystal ligand, was eliminated from the protein and polar hydrogen atoms were added to get the protonated protein crystal using autodock tools. All the active ligands were docked into the active pocket of this 15-LOX protein using the built-in united atom scoring function of autodock vina with 10 runs for each compound to find the best possible active configuration [55].

4.11.2. DFT calculations

Density functional theory (DFT) calculations were performed using the Guassian09 software. All the files were executed using the B3LYP functional scheme, and the 3-21G basis set. This B3LYP is an effective theory used in the DFT calculation to determine the electronic structure of atoms and molecules. In this process of DFT studies all the chemical structures of selected derivatives were depicted in ChemDraw 12.0. For the superficial energy reduction, ChemDraw 3D Pro was used. Along with the improved geometric parameters, FMOs, global, and local reactivity descriptors were derived. In order to analyze the results Guass View 6 was used [56–58].

4.11.3. MD simulations

To ascertain the binding interactions and stability of the ligand–-protein complex under accelerated circumstances, MD simulations were performed. Using Nano scale molecular dynamic (NAMD) software on a CUDA-accelerated GPU machine with a 16 core CPU and 64 GB RAM memory, a molecular dynamic simulation investigation of the top-ranked conformation was carried out. VMD software was utilized to visualize MD simulation results [59]. The most highly ranked ligand–-protein complex was chosen, and topology data for the protein and the ligand were created using the CHARMM36 forcefield [60]. Charges of NaCl were added to neutralize the system. To eliminate any near atomic interactions, the system was minimized to the sharpest energy gradient. The system was equilibrated in an NVT ensemble for 500,000 steps, followed by another 500,000 steps in an NPT ensemble. Afterward,

simulation was performed for 50 ns under periodic boundaries condition [61].

Declaration of competing interest

The authors declare that they have no known competing financial interests or personal relationships that could have appeared to influence the work reported in this paper.

Appendix A. Supplementary data

Supplementary data to this article can be found online at https://doi.org/10.1016/j.bioorg.2023.106984.

References

[1] H. Tallima, R.E. Ridi, Arachidonic acid: physiological roles and potential health benefits-A review, J. Adv. Res. 11 (2018) 33–41.

[2] U.P. Kelavkar, C. Cohen, H. Kamitani, T.E. Eling, K.F. Badr, Concordant induction of 15-lipoxygenase-1 and mutant p53 expression in human prostate adenocarcinoma: Correlation with Gleason staging, Carcinogenesis 21 (2000) 1777–1787.

[3] J. Zhu, I. Kilty, H. Granger, E. Gamble, Y.S. Qiu, K. Hattotuwa, W. Elston, W.L. Liu, A. Oliva, J.C. Kips, R.A. Pauwels, Gene expression and immunolocalization of 15-lipoxygenase isozymes in the airway mucosa of smokers with chronic bronchitis, Am. J. Respir. Cell Mol. Biol. 27 (2002) 666–677.

[4] E. Skrzypczak-Jankun, K. Zhou, N.P. McCabe, S.H. Selman, J. Jankun, Structure of curcumin in complex with lipoxygenase and its significance in cancer, Int. J. Mol. Med. 12 (2003) 17–24.

[5] X.Z. Ding, P. Iversen, M.W. Cluck, J.A. Knezetic, T.E. Adrian, Lipoxygenase inhibitors abolish proliferation of human pancreatic cancer cells, Biochem. Biophy. Res. Comm. 261 (1999) 218–223.

[6] D. Zhu, Y. Ran, Role of 15-lipoxygenase/15-hydroxyeicosatetraenoic acid in hypoxia-induced pulmonary hypertension, J. Physiol. Sci. 62 (2012) 163–172.

[7] F. Pagniez, N. Lebouvier, Y.M. Na, I. Ourliac-Garnier, C. Picot, M.L. Borgne, P. L. Pape, Biological exploration of a novel 1,2,4-triazole-indole hybrid molecule as antifungal agent, J. Enz. Inhib. Med. Chem. 35 (2020) 398–403.

[8] H.M.A. Asif, S. Kamal, A.U. Rehman, S. Rasool, M.S.H. Akash, Synthesis, characterization, and enzyme inhibition properties of 1,2,4-triazole bearing azinane analogues, ACS Omega 36 (2022) 32360–32368.

[9] S. El-Sebaey, Recent advances in 1,2,4-triazole scaffolds as antiviral agents, ChemSelect 37 (2020) 11654–11680.

[10] E. Gultekin, Y. Kolcuoglu, A. Akdemir, Y. Sirin, H. Bektas, O. Bekircan, A study on synthesis, biological activities and molecular modelling of some novel trisubstituted 1,2,4-triazole derivatives, ChemSelect 3 (2018) 8813–8818.

[11] S.A. El-Sebaey, Recent advances in 1,2,4-triazole scaffolds as antiviral agents, ChemSelect 5 (2020) 11654–11680.

[12] Y.Z. Sun, J.W. Wu, S. Du, Y.C. Ma, L. Zhou, Y. Ma, R.L. Wang, Design, synthesis, biological evaluation and molecular dynamics of LAR inhibitors, Comp. Biol. Chem. 92 (2021), 107481.

[13] M.R. Aouad, H.M. Al-Mohammadi, F.F. Al-Blewi, S. Ihmaid, H.M. Elbadawy, S. S. Althagfan, N. Rezki, Introducing of acyclonucleoside analogues tethered 1,2,4-triazole as anticancer agents with dual epidermal growth factor receptor kinase and microtubule inhibitors, Bioorg. Chem. 94 (2020), 103446.

[14] E. Guzel, U.A. Çevik, A.E. Evren, H.E. Bostancı, U.D. Gul, U. Kayış, Z. A. Kaplancıklı, Synthesis of benzimidazole-1,2,4-triazole derivatives as potential antifungal agents targeting 14-α-demethylase, ACS Omega 8 (2023) 4369–4384.

[15] O. Bekircan, N. Baltaş, E. Menteşe, E. Gultekin, Synthesis of new fluorine-containing 1,2,4-triazole-5-on derivatives with their anti-urease, anti-xanthine oxidase and antioxidant activities, Rev. Roum. Chim. 61 (2016) 733–746.

[16] Ł. Szczukowski, E. Krzyzak, B. Wiatrak, P. Jawien, A. Marciniak, A. Kotynia, P. Swiątek, New N-substituted-1,2,4-triazole derivatives of pyrrolo [3,4-d] pyridazinone with significant anti-inflammatory activity-Design, synthesis and complementary in vitro, computational and spectroscopic studies, Int. J. Mol. Sci. 22 (2021) 11235.

[17] W.A. Jawad, A.A. Balakit, M.N.A. Al-Jibouri, Y. Sert, M. Obies, Design, synthesis, characterization, antioxidant, antiproliferative activity and molecular docking studies of new transition metal complexes of 1,2,4-triazole as combretastatin A-4 analogues, J. Mol. Str. 127 (2023), 134437.

[18] D. Kumudha, R.R. Reddy, T. Kalavathi, Synthesis and evaluation of some 1,3,4-thiadiazoles having substituted 1,2,4-triazole moiety for anticonvulsant and CNS depressant activity, World J. Pharm. Pharm. Sci. 3 (2014) 728–740.

[19] J. Jiao, H. Xiang, Q. Liao, Recent advancement in nonsteroidal aromatase inhibitors for treatment of estrogen-dependent breast cancer, Cur. Med. Chem. 17 (2010) 3476–3487.

[20] P.H., Spiekermann, & M.D. Young, Clinical evaluation of clotrimazole: a broad-spectrum antifungal agent. Arch. Dermatol., 112 (1976) 350-352.

[21] Z. Song, Y. Liu, Z. Dai, W. Liu, K. Zhao, T. Zhang, Y. Dai, Synthesis and aromatase inhibitory evaluation of 4-N-nitrophenyl substituted amino-4H-1,2,4-triazole derivatives, Bioorg. Med. Chem. 24 (2016) 4723–4730.

[22] U.A. Çevik, B.K. Çavuşoglu, B.N. Saglık, D. Osmaniye, S. Levent, S. Ilgın, Z. A. Kaplancıklı, Synthesis, docking studies and biological activity of new benzimidazole-triazolothiadiazine derivatives as aromatase inhibitor, Molecules 25 (2020) 1642.

[23] N. Akhter, S. Batool, S.G. Khan, N. Rasool, F. Anjum, A. Rasul, S. Imran, Bio-oriented synthesis and molecular docking studies of 1,2,4-triazole based derivatives as potential anti-cancer agents against HepG2 Cell Line, Pharmaceuticals 16 (2023) 211.

[24] L. Emami, S. Sadeghian, A. Mojaddami, S. Khabnadideh, H. Sakhteman, Z. Sadeghpour, M.F. Faghih, Z. Rezaei, Design, synthesis and evaluation of novel 1,2,4-triazole derivatives as promising anticancer agents, BMC Chem. 16 (2022) 91, https://doi.org/10.1186/s13065-022-00887-x.

[25] M.M. Alanazi, A. Elwan, N.A. Alsaif, A.J. Obaidullah, H.M. Alkahtani, A.A. Al-Mehizia, S.M. Alsubaie, M.S. Taghour, I.H. Eissa, Discovery of new 3-methylquinoxalines as potential anti-cancer agents and apoptosis inducers targeting VEGFR-2: Design, synthesis, and in silico studies, J. Enz. Inhib. Med. Chem. 36 (2021) 1732–1750.

[26] R. Aggarwal, G. Sumran, An insight on medicinal attributes of 1,2,4-triazoles, Eur. J. Med. Chem. 205 (2020), 112652.

[27] F.H. Al-Ostoot, M. Al-Ghorbani, S.A. Khanum, Recent investigation on heterocycles with one nitrogen [piperidine, pyridine and quinoline], two nitrogen [1,3,4-thiadiazole and pyrazole] and three nitrogen [1,2,4-triazole]: a review, J. Iranian Chem. Soc. 19 (2022) 23–54.

[28] A. Rafique, S. Muhammad, J. Iqbal, A.G. Al-Sehemi, M.Y. Alshahrani, K. Ayub, M. A. Gilani, Exploring the inhibitory potential of novel piperidine-derivatives against main protease (Mpro) of SARS-CoV-2: A hybrid approach consisting of molecular docking, MD simulations and MMPBSA analysis, J. Mol. Liq. 382 (2023), 121904.

[29] D.J. Calleja, N. Kuchel, B.G. Lu, R.W. Birkinshaw, T. Klemm, M. Doerflinger, D. Komander, Insights into drug repurposing, as well as specificity and compound properties of piperidine-based SARS-CoV-2 PLpro Inhibitors, Front. Chem. 10 (2022), 861209.

[30] D. De Lucia, O.M. Lucio, B. Musio, A. Bender, M. Listing, S. Dennhardt, S.V. Ley, Design, synthesis and evaluation of semi-synthetic triazole-containing caffeic acid analogues as 5-lipoxygenase inhibitors, Eur. J. Med. Chem. 101 (2015) 573–583.

[31] M.G. Chini, R.D. Simone, I. Bruno, R. Riccio, F. Dehm, C. Weinigel, G. Bifulco, Design and synthesis of a second series of triazole-based compounds as potent dual mPGES-1 and 5-lipoxygenase inhibitors, Eur. J. Med. Chem. 54 (2012) 311–323.

[32] P.A. Elzahhar, S.M. Abd El Wahab, M. Elagawany, H. Daabees, A.S. Belal, A.F. El-Yazbi, C.T. Supuran, Expanding the anticancer potential of 1,2,3-triazoles via simultaneously targeting cyclooxygenase-2, 15-lipoxygenase and tumor-associated carbonic anhydrases, Eur. J. Med. Chem. 200 (2020), 112439.

[33] A.M. Mohassab, H.A. Hassan, D. Abdelhamid, A.M. Gouda, H.A. Gomaa, B. G. Youssif, M. Abdel-Aziz, New quinoline/1,2,4-triazole hybrids as dual inhibitors of COX-2/5-LOX and inflammatory cytokines: Design, synthesis, and docking study, J. Mol. Str. 1244 (2021), 130948.

[34] W. Shahid, M. Ashraf, M. Saleem, B. Bashir, S. Muzaffar, M. Ali, A. Kaleem, H. Aziz-ur-Rehman, K. Amjad, N.R. Bhattarai, Exploring phenylcarbamoylazinane-1,2,4-triazole thioethers as lipoxygenase inhibitors supported with expression analysis, cellular viability and *in silico* studies, Bioorg. Chem. 115 (2021), 105261.

[35] N. Riaz, M. Yasin, M. Ashraf, M. Saleem, B. Bashir, A. Iqbal, S.A. Aziz-ur-Rehman, H.M.K. Ejaz, K.B. Mahmood, Vetting of new *N*-furfurylated *p*-chlorophenyl-1,2,4-triazole acetamides as lipoxygenase inhibitors assisted with in vitro and in silico studies, J. Iranian Chem. Soc. 20 (2023) 1–18.

[36] B. Bashir, W. Shahid, M. Ashraf, M. Saleem, S. Aziz-ur-Rehman, M. Muzaffar, H. Imran, K. Amjad, N.R. Bhattarai, Identification of phenylcarbamoylazinane-1,3,4-oxadiazole amides as lipoxygenase inhibitors with expression analysis and computational studies, Bioorg. Chem. 115 (2021), 105243.

[37] B. Bashir, N. Riaz, S.A. Ejaz, M. Saleem, M. Ashraf, A. Iqbal, S. Muzaffar, H.M. K. Mahmood, K. Bhattarai, Assessing *p*-tolyloxy-1,3,4-oxadiazole acetamides as lipoxygenase inhibitors assisted by in vitro and in silico studies, Bioorg. Chem. 129 (2022), 106144.

[38] B. Bashir, N. Riaz, S.A. Ejaz, M. Saleem, A. Iqbal, M. Ashraf, A. Aziz-ur-Rehman, K. B. Saeed, Parsing *p*-tolyloxy-1,3,4-oxadiazolemethylacetamides as 15-lipoxygenase inhibitors prop up by in vitro and in silico profiling, J. Mol. Str. 1275 (2022), 134664.

[39] B. Bashir, N. Riaz, S.A. Ejaz, M. Saleem, A. Iqbal, M. Ashraf, S. Ejaz, M. Aziz-ur-Rehman, K.B. Aziz, Investigations of *p*-tolyloxy-1,3,4-oxadiazole propionamides as soybean 15-lipoxygenase inhibitors in comforting with in vitro and in silico studies, J. Biomol. Struct. Dyn. (2023), https://doi.org/10.1080/07391102.2023.2190807.

[40] M. Yasin, W. Shahid, M. Ashraf, M. Saleem, S. Muzaffar, S.A. Aziz-ur-Rehman, A. Ejaz, T. Saeed, K. Majer, N.R. Bhattarai, 4-Chlorophenyl-N-furfuryl-1,2,4-triazole methylacetamides as significant 15-lipoxygenase inhibitors: An efficient approach for finding lead anti-inflammatory compounds. ACS, Omega 7 (2022) 19721–19734.

[41] M. Yasin, W. Shahid, M. Ashraf, M. Saleem, S. Muzaffar, S.A. Aziz-ur-Rehman, H. M.K. Ejaz, K.B. Mahmood, N. Riaz, Targeting new N-furfurylated 4-chlorophenyl-1,2,4-triazolepropionamide hybrids as potential 15-lipoxygenase inhibitors supported with in vitro and in silico studies, J. Biomol. Str. Dyn. 41 (2023) 5166–5182.

[42] C.A. Lipinski, F. Lombardo, B.W. Dominy, P.J. Feeney, Experimental and computational approaches to estimate solubility and permeability in drug discovery and development settings, Adv. Drug Deliv. Rev. 23 (1997) 3–25.

[43] D.F. Veber, S.R. Johnson, H.-Y. Cheng, B.R. Smith, K.W. Ward, K.D. Kopple, Molecular properties that influence the oral bioavailability of drug candidates, J. Med. Chem. 45 (2002) 2615–2623.

[44] O. Trott, A.J. Olson, AutoDock Vina: improving the speed and accuracy of docking with a new scoring function, efficient optimization, and multithreading, J. Comp. Chem. 31 (2010) 455–461.
[45] S. Abbas, S. Zaib, S. Ali, J. Iqbal, 15-LOX Inhibitors: Biochemical evaluation of flurbiprofen and its derivatives, Life Sci. 1 (2020) 92–97.
[46] L.I. Design, Pharmacophore and ligand-based design with Biovia Discovery Studio®, Biovia, California, 2014.
[47] V.A. Rassolov, J.A. Pople, M.A. Ratner, T.L. Windus, 6–31G* basis set for atoms K through Zn, The J. Chem. Phy. 109 (1998) 1223–1229.
[48] A. Frisch, Gaussian 09W Reference. Wallingford, USA, 25p. (2009) 470.
[49] K. Liu, H. Kokubo, Exploring the stability of ligand binding modes to proteins by molecular dynamics simulations: a cross-docking study, J. Chem. Inform. Model. 57 (2017) 2514–2522.
[50] M. Ans, J. Iqbal, B. Eliasson, K. Ayub, Opto-electronic properties of non-fullerene fused-undecacyclic electron acceptors for organic solar cells, Comp. Mat. Sci. 159 (2019) 150–159.
[51] M.A. Erteeb, E.E. Ali-Shattle, S.M. Khalil, H.A. Berbash, Z.E. Elshawi, Computational studies (DFT) and PM3 theories on thiophene oligomers as corrosion inhibitors for iron, Am. J. Chem. 11 (2021) 1–7.
[52] B.S. Kedare, R.P. Singh, Genesis and development of DPPH method of antioxidant assay, J. Food Sci. Technol. 48 (2011) 412–422.
[53] P.W. Rose, A. Prlić, A. Altunkaya, C. Bi, A.R. Bradley, C.H. Christie, L.D. Costanzo, J.M. Duarte, S. Dutta, Z. Feng, R.K. Green, D.S. Goodsell, B. Hudson, T. Kalro, R. Lowe, E. Peisach, C. Randle, A.S. Rose, C. Shao, Y. Yi-Ping Tao, M. Valasatava, J. D. Voigt, J. Westbrook, H. Woo, J.Y. Yang, C. Young, H.M. Zardecki, S.K. B. Berman, The RCSB protein data bank: integrative view of protein, gene and 3D structural information, Nucleic Acids Res. 45 (2017) D271–D281.
[54] R. Huey, G.M. Morris, S. Forli, Using AutoDock 4 and AutoDock vina with AutoDockTools: a tutorial, The Scripps Research Institute Molecular Graphics Laboratory 10550 (92037) (2012) 1000.
[55] M.J. Frisch, G.W. Trucks, H.B. Schlegel, G. E. Scuseria, M.A. Robb, J.R. Cheeseman, G. Scalmani, V. Barone, B. Mennucci, G.A. Petersson, H. Nakatsuji, M. Caricato, X. Li, H.P. Hratchian, A.F. Izmaylov, J. Bloino, G. Zheng, J.L. Sonnenberg, M. Hada, M. Ehara, K. Toyota, R. Fukuda, J. Hasegawa, M. Ishida, T. Nakajima, Y. Honda, O. Kitao, H. Nakai, T. Vreven, J.A. Montgomery, Jr., J.E. Peralta, F. Ogliaro, M. Bearpark, J.J. Heyd, E. Brothers, K.N. Kudin, V.N. Staroverov, T. Keith, R. Kobayashi, J. Normand, K. Raghavachari, A. Rendell, J.C. Burant, S.S. Iyengar, J. Tomasi, M. Cossi, N. Rega, J.M. Millam, M. Klene, J.E. Knox, J.B. Cross, V. Bakken, C. Adamo, J. Jaramillo, R. Gomperts, R.E. Stratmann, O. Yazyev, A.J. Austin, R. Cammi, C. Pomelli, J.W. Ochterski, R.L. Martin, K. Morokuma, V.G. Zakrzewski, G. A. Voth, P. Salvador, J.J. Dannenberg, S. Dapprich, A.D. Daniels, O. Farkas, J.B. Foresman, J.V. Ortiz, J. Cioslowski, D.J. Fox, Gaussian, Inc., Wallingford CT, 2010.
[56] L. Goerigk, J.R. Reimers, Efficient methods for the quantum chemical treatment of protein structures: the effects of London-dispersion and basis-set incompleteness on peptide and water-cluster geometries, J. Chem. Theory Comput. 9 (2013) 3240–3251.
[57] GaussView, Version 6, Roy Dennington, T.A. Keith, J.M. Millam, Semichem Inc., Shawnee Mission, KS, (2016).
[58] K.J. Bowers, E. Chow, H. Xu, R.O. Dror, M.P. Eastwood, B.A. Gregersen, J.L. Klepeis, I. Kolossvary, M.A. Moraes, F.D. Sacerdoti, J.K. Salmon, Y. Shan, D.E. Shaw, Scalable algorithms for molecular dynamics simulations on commodity clusters, SC '06: Proceedings of the 2006 ACM/IEEE conference on supercomputing. (2006) 43-43.
[59] L.G. Ferreira, R.N. Dos Santos, G. Oliva, A.D. Andricopulo, Molecular docking and structure-based drug design strategies, Molecules 20 (2015) 13384–13421.
[60] P.W. Hildebrand, A.S. Rose, J.K. Tiemann, Bringing molecular dynamics simulation data into view, Trends Biochem. Sci. 44 (2019) 902–913.